Open Access

Recent Progress in Materials

LIDSEN Publishing Inc.

Original Research

Micromechanics-Based Modeling of SiC/SiC Ceramic Matrix Composites and Structures

Subodh K. Mital [1], Steven M. Arnold [2, *], Brett A. Bednarcyk [2], Evan J. Pineda [2]

1. The University of Toledo, Toledo, Ohio 43606, USA; E-Mail: subodh.k.mital@nasa.gov
2. NASA Glenn Research Center, Cleveland, Ohio 44135, USA; E-Mails: Steven.M.Arnold@nasa.gov; brett.a.bednarcyk@nasa.gov; evan.j.pineda@nasa.gov

* **Correspondence:** Steven M. Arnold; E-Mail: Steven.M.Arnold@nasa.gov

Academic Editor: Ali Abdul-Aziz

Special Issue: Ceramic Matrix Composites: Performance Evaluation and Application

Recent Progress in Materials
2023, volume 5, issue 2
doi:10.21926/rpm.2302025

Received: January 23, 2023
Accepted: June 05, 2023
Published: June 20, 2023

Abstract

The behavior and response of ceramic matrix composites (CMCs), in particular silicon carbide fiber reinforced silicon carbide matrix (SiC/SiC), is affected by many factors such as variation of fiber volume fraction, residual stresses resulting from processing of the composites at high temperature, random microstructures, and the presence of matrix flaws (e.g., voids, pores, cracks etc.) as well as general material nonlinearity and heterogeneity that occurs randomly in a composite. Residual stresses arising from the phase change of constituents are evaluated in this paper and it is shown that they do influence composite strength and need to be properly accounted for. Additionally, the microstructures (location of fiber centers, coating thickness etc.) of advanced CMCs are usually disordered (or random) and fiber diameter and strength typically have a distribution. They rarely resemble the ordered fiber packing (square, rectangular, or hexagonal) that is generally assumed in micromechanics-based models with periodic boundary conditions for computational expediency. These issues raise the question of how should one model such systems effectively? Can an ordered hexagonal packed repeating unit cell (RUC) accurately represent the random microstructure behavior? How many fibers need to be included to enable accurate representation? Clearly, the number of

fibers within an RUC must be limited to insure a balance between accuracy and efficiency. NASA's in-house micromechanics-based code MAC/GMC provides a framework to analyze such RUCs for the overall composite behavior and the FEAMAC computer code provides linkage of MAC/GMC to the commercial FEA code, ABAQUS. The appropriate level of discretization of the RUC as well as the analysis method employed, i.e., Generalized Method of Cells (GMC) or High Fidelity Generalized Method of Cells (HFGMC), is investigated in this paper in the context of a unidirectional as well as a cross-ply laminated CMC. Results including effective composite properties, proportional limit stress (an important design parameter) and fatigue are shown utilizing both GMC as well as HFGMC. Finally, a few multiscale analyses are performed on smooth bar test coupons as well as test coupons with features such as open-hole and double notches using FEAMAC. Best practices and guidance are provided to take these phenomena into account and keep a proper balance between fidelity (accuracy) and efficiency. Following these guidelines can account for important physics of the problem and provide significant advantages when performing large multiscale composite structural analyses. Finally, to demonstrate the multiscale analysis framework, a CMC gas turbine engine vane structure is analyzed involving a progressive damage model.

Keywords
Micromechanics; ceramic matrix composites; deformation; damage; fatigue; multiscale modeling

1. Introduction

Advanced ceramic matrix composites (CMCs) are being aggressively pursued as potential candidates for many aerospace applications as they offer a unique combination of high temperature strength, creep resistance, low density, high thermal conductivity, and low thermal expansion. Residual stresses can occur in CMCs due to the difference in coefficient of thermal expansion (CTE) of various constituents, ply layers and/or constituent phase changes within the composite. Since both fiber and matrix are silicon carbide based, the CTE mismatch is usually minimal. In melt-infiltrated (MI) SiC/SiC composites, the preform is infiltrated with molten silicon to create a dense composite. The silicon reacts with carbon in the preform to create a reaction-formed silicon carbide (SiC) matrix. However, there is always some excess silicon in the matrix, referred to as free silicon. This free silicon goes through a phase change during the processing of the composite and results in residual stresses in the as-fabricated composite. The resulting residual stress influences both the composite proportional limit stress (PLS) as well as the ultimate tensile strength (UTS). PLS, also referred to as the matrix-cracking stress is a very important design parameter since matrix cracks provide a path for the atmosphere to degrade the fiber matrix interface and fiber strength. It is believed that PLS will be the upper limit of the allowable CMC stress for long life applications [1].

Low fiber volume fraction composite systems like CMCs inherently have more microstructure variations (location of fiber centers – disordered/random packing, coating thickness, etc.) than higher volume fraction polymer matrix composite (PMC) systems. In addition, there is manufacturing variability along the fiber length, such as variable fiber diameter and variable

thickness of fiber coatings, thus raising the question of how one should model such systems effectively, i.e., keeping a proper balance between accuracy and efficiency when performing multiscale composite analyses. Clearly, from a computational point of view, it is preferable to keep the number of fibers in a repeating unit cell (RUC) to a minimum. NASA's in-house micromechanics-based code MAC/GMC [2], which has now evolved into NASMAT (NASA Multiscale Analysis Tool) [3], provides a framework to analyze such RUCs for the overall composite behavior. This framework embodies two basic micromechanics models, 1) Generalized Method of Cells (GMC) and 2) High Fidelity Generalized Method of Cells (HFGMC), which provide semi closed-form constitutive equations for composite effective properties, composite response, as well as local (microscale) stress and strain fields in the constituents of the composite. With the increased emphasis on reducing the cost and time to market of new materials, multiscale analyses [4-10], where the analyses span across various length scales in an integrated manner, and Integrated Computational Materials Engineering (ICME) are becoming a fast-growing discipline within materials science and engineering [11-14]. ICME is an integrated approach to the design of products and the materials which comprise them by linking material models at multiple time and length scales; such that manufacturing processes, which produce internal material structures that in turn influence material properties and design allowables, can be tailored (engineered) to specific industrial applications. Experimental micrographs of composite microstructures have shown that actual microstructures rarely resemble ordered arrangements and show at least some degree of spatial randomness, although this randomness diminishes as fiber volume fraction increases since fiber movement is more constrained (see Figure 1). However, due to the diminishing effect of microscale randomness at higher length scales, microstructural variability is often ignored and micromechanics-based models assuming periodic boundary conditions, with an ordered array of fibers (either square or hexagonally packed fibers), are typically utilized.

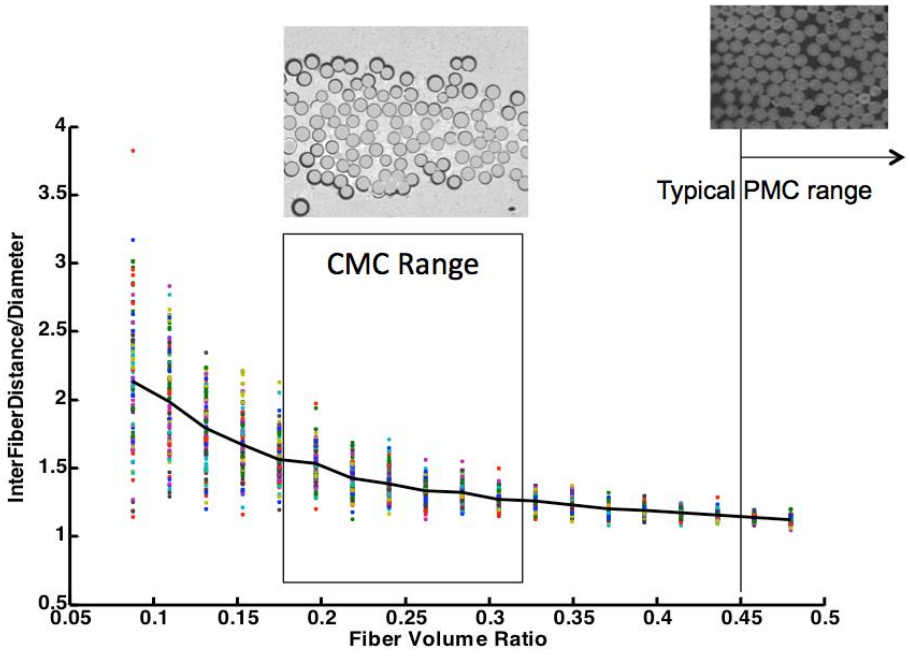

Figure 1 Measure of fiber movement versus fiber volume fraction. Micrograph for a typical ceramic matrix composite.

Researchers have investigated the effect of random or disordered microstructures on various composite response behaviors, assuming elastic and damage behavior [15-21]. In our previous work [22], the influence of ordered and disordered microstructures on the effective properties and fatigue life of graphite/epoxy polymer matrix composite (PMC) at low volume fractions was studied in the context of assessing the advantages/limitations of the micromechanics idealizations (GMC - generalized method of cells or HFGMC – high fidelity generalized method of cells) available within the general, synergistic, multiscale-modeling framework for composites (developed by the NASA Glenn Research Center (GRC)) and known as MAC/GMC and FEAMAC [23] when considering microstructural arrangement. This framework can be effectively utilized to link the material microstructure (e.g., constituent phase properties, volume fraction, fiber packing) to ply/laminate properties (mesoscale) and finally to performance (at the macroscale), see Figure 2, in an efficient and accurate manner to enable 'fit-for-purpose' tailoring of the composite material. Finally, a few micromechanics-based multiscale analyses are performed on smooth bar test coupons as well as open-hole and double-notched unidirectional and cross-ply test coupons. Since these analyses are usually quite resource intense, recommendations are made for selection of a proper RUC with regards to size and details included, as well as the analysis method used. The desire again is to maintain a proper balance between accuracy (fidelity of the model) and efficiency for achieving practical engineering results in a reasonable amount of time to make the tool practical.

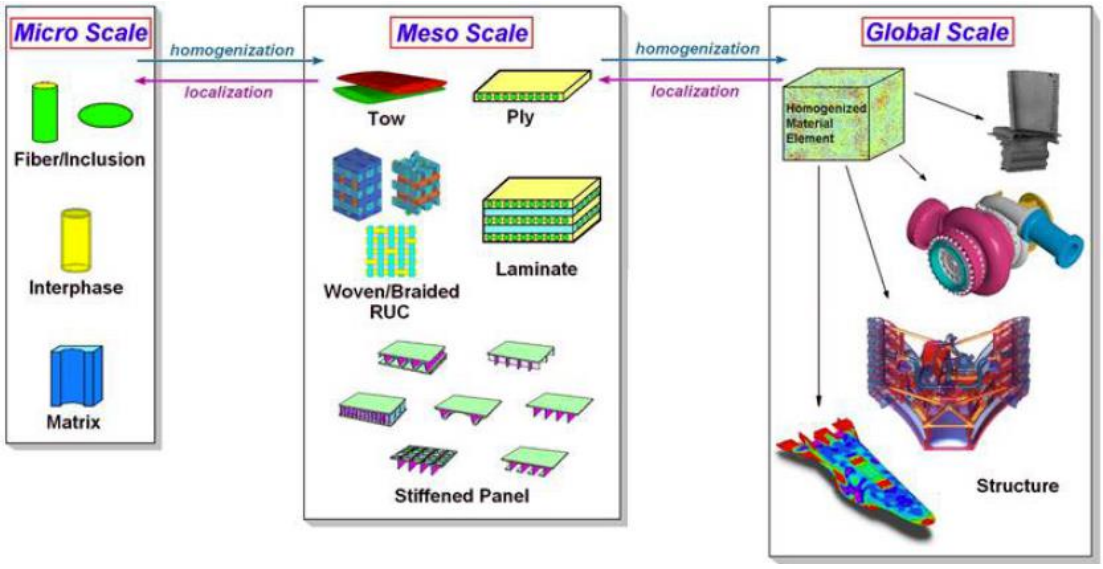

Figure 2 Illustration of relevant levels of scales for multiscale composite analysis.

The objective of this paper is to summarize our current understanding of: the effect of residual stresses on the composite response, the statistical influence of microstructure (both ordered and disordered) on the overall accuracy of predicted unidirectional and laminated CMCs response for both static and cyclic loading, the advantages/limitations of the micromechanics idealization (GMC or HFGMC), and the influence of lower length scale idealizations on higher scale response in multiscale analyses. A brief background of the generalized method of cells along with details of the continuum damage fatigue model employed are presented in the following sections. Residual stresses that arise due to processing are discussed and a general discussion of the RUC based modeling of the ordered and disordered microstructure is presented next. Results for elastic

properties, strength and fatigue lives using two micromechanics theories available in MAC/GMC computer code as well as effects of manufacturing variability arising due to the variation in fiber diameter and interface coating thickness are presented next. The paper concludes with some multiscale problems that demonstrate the capability of the MAC/GMC and FEAMAC computer code along with some general concluding remarks.

2. Generalized Method of Cells

GMC, first developed by Paley and Aboudi [24] and HFGMC, first developed by Aboudi et al. [23], are semi-analytical in nature, and their formulation involves application of several governing conditions in an average sense. They provide the local fields in composite materials, allowing incorporation of arbitrary inelastic constitutive models with various deformation and damage constitutive laws [23]. The microstructure of a periodic multiphase material, within the context of GMC and HFGMC, is represented by a doubly periodic (continuously reinforced) or triply periodic (discontinuously reinforced) RUC consisting of an arbitrary number of subcells, each of which may be a distinct material (Figure 3). In the case of GMC, the displacement field is assumed linear, whereas in the case of HFGMC the displacement approximations are assumed quadratic, thus leading to a constant and linear subcell strain field, respectively. In fact, it is precisely this higher order assumption in the displacement field that enables HFGMC to retain its ability to compute nonzero transverse shear stress distributions within the composite (i.e., normal and shear coupling), which is so important when dealing with disordered microstructures [25]. However, it is also this high-order field assumption which makes HFGMC more computationally expensive [26] and subject to subcell discretization dependence as compared to GMC.

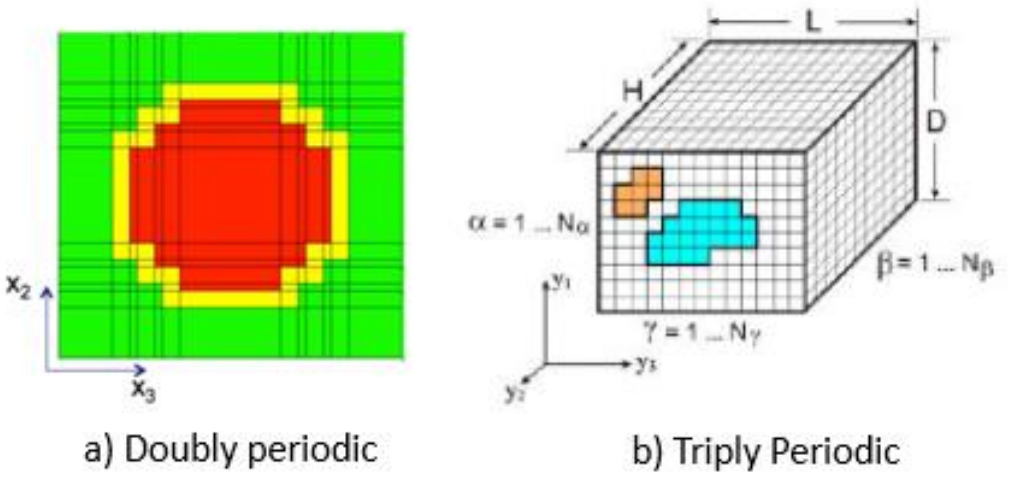

Figure 3 Composite with repeating microstructure and arbitrary constituents.

Displacement and traction continuity are enforced in an average, or integral sense at each of the subcell interfaces and the periodic boundaries of the RUC. These continuity conditions are used to formulate a strain concentration matrix A, which gives all the local subcell strains (ϵ_S) in terms of the global, average, applied strains $\epsilon_{applied}$ (i.e., $\epsilon_S = A\epsilon_{applied}$). The local subcell stresses (σ) can then be calculated using the local constitutive law and the local subcell strains. Finally, the overall RUC stiffness is obtained utilizing the local constitutive law and the strain concentration matrix averaged

over the RUC dimensions. The detailed methodology of GMC and HFGMC and the formulation to be embedded within classical laminate theory is described thoroughly in Aboudi et al. [23, 27]. Also, in these references the superior accuracy of HFGMC over that of GMC is demonstrated, consequently in this study HFGMC will be assumed to provide the most accurate predictions.

3. Constitutive Models

The most well-known and widely used constitutive model, Hooke's law, is written as

$$\sigma_{ij} = C_{ijkl}\varepsilon_{kl} \tag{1}$$

which describes time-independent, linear (proportional) reversible material behavior, where C_{ijkl} is the classic stiffness tensor and ε_{kl} is the elastic component of the strain tensor. Extension into the irreversible regime has been accomplished by assuming an additive decomposition of the total strain tensor into three components, that is a reversible mechanical strain (i.e., elastic/viscoelastic) ε_{ij}; an irreversible (i.e., inelastic or viscoplastic) strain ε_{ij}^{I}; and a reversible thermal strain, ε_{ij}^{th} component.

$$\varepsilon_{ij}^{total} = \varepsilon_{ij} + \varepsilon_{ij}^{I} + \varepsilon_{ij}^{th} \tag{2}$$

or

$$\varepsilon_{ij} = \varepsilon_{ij}^{total} - \varepsilon_{ij}^{I} - \varepsilon_{ij}^{th} \tag{3}$$

After substituting expression (3) into equation (1) we arrive at a stress strain relation (generalized Hooke's law) that incorporates irreversible strains as well as reversible ones, that is:

$$\sigma_{ij} = C_{ijkl}\left(\varepsilon_{kl} - \varepsilon_{kl}^{I} - \varepsilon_{kl}^{th}\right) \tag{4}$$

where numerous models describing the evolution of the inelastic strain have been proposed in the literature (e.g., [23, 28-30]).

3.1 Deformation Model

Constituent deformation behavior is assumed to follow Hooke's Law up to failure. The elastic properties of all three constituent materials (Hi-Nicalon Type-S fiber, BN coating and SiC matrix) are given in Table 1. These properties have been assumed based on internal discussions with the ceramic materials researchers. The matrix (represented by green subcells), the fiber (represented by red subcells) and the explicit interface coating (represented by yellow subcells) in Figure 3a are all assumed isotropic; with Young's modulus (E_m, E_f, E_c) and Poisson's ratio (ν_m, ν_f, ν_c) along with the associated shear modulus (G_m, G_f, G_c) all given in Table 1. Note the ratio of constituent properties are $E_f/E_m = 1.18$; $E_c/E_m = 0.03$; $G_f/G_m = 1.23$; $G_c/G_m = 0.03$. This is important because the mismatch in constituent properties effects the stress redistribution within a composite. All constituents are assumed to be brittle, and the static failure of each constituent is assumed to be governed by the maximum stress criterion (both normal (σ_u) and shear (τ)) with the strengths given in Table 1. The proportional limit stress (PLS) is determined from the global stress-strain curve by assuming the CMC community accepted 0.005 percent total strain off-set from the origin. Temperature

dependent constituent elastic and creep properties are given in Table 2 wherein creep (ε_{ij}^{I}) is idealized using an isotropic Norton-Bailey power law creep model [30]. Norton-Bailey power law for uniaxial creep can be written as:

$$\frac{d\varepsilon^{I}}{dt} = A\sigma^{n} \tag{5}$$

where A and n are required isotropic parameters of this model, σ is the stress and t is time. A multiaxial form of this law, known as Odqvist [31] model can be written as:

$$\frac{d\varepsilon_{ij}^{I}}{dt} = BJ_2^{m}S_{ij} \tag{6}$$

where $m = \frac{1}{2}(n-1)$ and $B = \frac{1}{2}\left(3^{\frac{n+1}{2}}\right)A$ and $J_2 = \frac{1}{2}S_{ij}S_{ij}$ with $S_{ij} = \sigma_{ij} - \frac{1}{3}\sigma_{kk}\delta_{ij}$.

Table 1 Constituent (fiber/matrix/coating) elastic properties.

Hi-Nicalon Type S Fiber	BN - Coating	SiC Matrix
E_f = 385.0 GPa	E_c = 10.0 GPa	E_m = 327.0 GPa
ν_f = 0.17	ν_c = 0.23	ν_m = 0.22
G_{f23} = 164.53 GPa	G_{c23} = 4.07 GPa	G_{m23} = 134.0 GPa
σ_{uf} = 1800 MPa	σ_{uc} = 70 MPa	σ_{um} = 600 MPa
τ_f = 700 MPa	τ_c = 45 MPa	τ_m = 350 MPa

Table 2 Temperature dependent constituent material properties.

Model Parameter	**Units**	**RT**	**1100°C**	**1200°C**	**1300°C**	**1400°C**
Hi-Nic Type S Fiber						
Young's Modulus, E	GPa	385.0	375.0	370.0	365.0	365.0
Poisson's Ratio, v_{12}		0.17	0.17	0.17	0.17	0.17
Coefficient of Thermal Expansion, α	10^{-06}/°C	3.2	5.5	5.5	5.5	5.5
A	MPa^{-3} hr	0	3.32×10^{-17}	1.68×10^{-13}	2.76×10^{-13}	5.17×10^{-13}
n		3	3	3	3	3
BN - Coating						
Young's Modulus, E	GPa	10	9	9	9	9
Poisson's Ratio, v_{12}		0.22	0.22	0.22	0.22	0.22
Coefficient of Thermal Expansion, α	10^{-06}/°C	4.0	5.5	5.5	5.5	5.5
SiC Matrix						
Young's Modulus, E	GPa	410.0	400.0	390.0	385.0	380.0
Poisson's Ratio, v_{12}		0.17	0.17	0.17	0.17	0.17
Coefficient of Thermal Expansion, α	10^{-06}/°C	3.1	5.5	5.5	5.5	5.5
A	MPa^{-3} hr	0	2.55×10^{-11}	2.04×10^{-09}	1.02×10^{-08}	4.31×10^{-08}

n		1.5	1.5	1.5	1.5	1.5
Free Silicon						
Young's Modulus, E	GPa	160.0	155.0	153.0	150.0	150.0
Poisson's Ratio, v_{12}		0.24	0.24	0.24	0.24	0.24
Coefficient of Thermal Expansion, α	10^{-06}/°C	3.0	6.0	6.0	6.0	6.0
A	MPa^{-3} hr	0	5.08×10^{-10}	4.06×10^{-08}	2.03×10^{-07}	8.6×10^{-07}
n		1.3	1.3	1.3	1.3	1.3

A(T) and n are creep parameters

As shown, the parameters of the multiaxial creep law can be computed from the parameters of the uniaxial creep model *A* and *n*. MAC/GMC uses the multiaxial form of the creep law. It should also be noted that monotonic failure is accounted for with the failure stress shown in Table 1 using the max. stress failure criterion. The explicit micro damage mechanisms that can be modeled are fiber failure, matrix failure and interfacial debonding. Once a material in a subcell fails, it stiffness is reduced to near zero if using the max. stress/strain criterion and the homogenization up through the scales brings this effect to the macro level. The macro level effective thermal and inelastic strains can be obtained in a similar fashion.

3.2 Continuum Fatigue Damage Model

Prediction of fatigue damage and fatigue life in fiber-reinforced ceramic-matrix composites under thermomechanical loading are of critical importance in the reliability and safe design of advanced aerospace structures. There are many fatigue models in the literature that can broadly be divided into two categories: (a) phenomenological models, including fatigue life models, residual strength model, and residual stiffness model, and (b) progressive damage models correlated with macroscopic residual mechanical properties and mesoscopic damage mechanisms [32, 33]. MAC/GMC utilizes a phenomenological micromechanics-based isotropic form of the multiaxial, isothermal, continuum damage mechanics model of Arnold and Kruch [34] for the matrix constituent. When reduced to its isotropic form this model reduces to the Non-Linear Cumulative Damage Rule (NLCDR) developed at the Office national d'études et de recherches aérospatiales (ONERA)- the French national aerospace research centre [35]. This model assumes a single scalar internal damage variable, *D*, that has a value of zero for undamaged material and one for a completely damaged (failed) material. The implementation of the damage model within GMC and HFGMC has been performed on the local scale, thus damage evolves in each subcell based on the local stress state and number of cycles. For a given damage level, the stiffness of the subcell is degraded by (1 - *D*). Further, the implementation allows the application of a local damage increment ΔD, and then calculates the number of cycles, *N*, required to achieve this local increment of damage. This approach allows the model to determine the stress state in the composite, identify the controlling subcell that will reach the desired damage level in the fewest cycles, apply that number of cycles to all subcells, and calculate the damage that arises throughout the remainder of the composite. Then the composite can be reanalyzed, and a new stress state determined based on the new, spatially varying, damage level throughout the composite RUC. In this way, the local and global

stress and damage analyses are coupled. As the damage in the composite evolves, the stress field in the composite is redistributed, which then affects the evolution of damage.

For an isotropic material, the damage parameters that must be selected reduce to *M*, β and *a*, while the pertinent equation relating the fatigue life of the isotropic material to the cyclic stress state is,

$$N_F = \frac{(\sigma_u - \sigma_{max})\left(\frac{M}{\sigma_{max} - \bar{\sigma}}\right)^{\beta}}{\hat{a}(1+\beta)\left(\sigma_{max} - \bar{\sigma} - \sigma_{fl}\right)} \quad for \quad N_F > 0 \tag{7}$$

Where σ_u is the material ultimate strength, σ_{fl} is the material fatigue limit (stress below which damage does not occur), σ_{max} is the maximum stress during a loading cycle, $\bar{\sigma}$ is the mean stress during a loading cycle, and N_F is the number of cycles to failure. Note that, in the terminology of Arnold and Kruch [34], $\hat{a} = a\frac{\sigma_{fl}}{\sigma_u}$. Utilizing equation (5), the damage model parameters *M*, β and a can be selected for an isotropic material based on the material's S-N curve (stress level vs. cycles to failure). Both the fatigue limit and the scaling parameter M are general enough to account for the effect of mean stress. However, in this study this additional effect is ignored since only one R ratio (R = -1, fully reversed) is examined. A representative S-N curve for a SiC matrix was obtained, and the corresponding fatigue damage model parameters were found to be *M* = 550 MPa, β = 8, and a = 0.4, with σ_u = 600 MPa, and σ_{fl} = 65.0 MPa. A plot showing the resulting matrix S-N curve is given in Figure 4. Note the dotted line illustrates how the above function behaves below a single cycle yet static fracture would occur at 600 MPa (as indicated by the x in Figure 4).

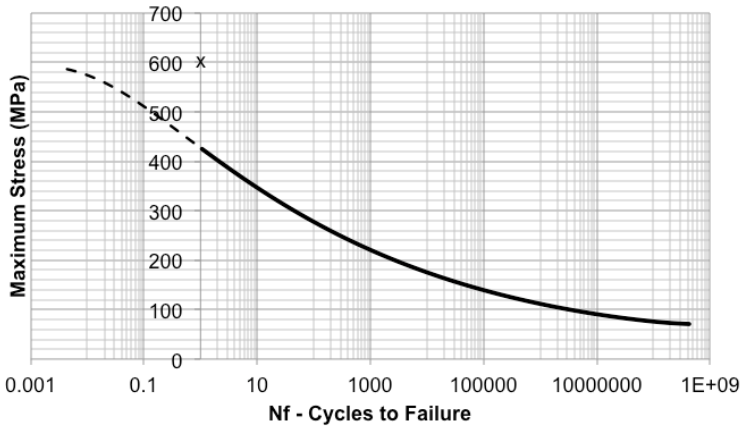

Figure 4 Stiffness reduction fatigue damage model representation for in-situ SiC matrix.

A second damage model within GMC and HFGMC is much simpler and involves degradation of a material's strength due to cyclic loading. As shown by Wilt et al. [36], this type of damage model can be used to simulate the fatigue behavior of fibers that occurs in-situ during fatigue of a composite. The model assumes a logarithmic relation between the material's strength and the number of cycles within a certain range such that:

$$\sigma_u = \sigma_{u1} \qquad 0 \le N \le N_1$$

$$\sigma_u = \sigma_{u1} - \frac{(\sigma_{u1} - \sigma_{u2})\log(N/N_1)}{\log(N_2/N_1)} \qquad N_1 \le N \le N_2 \tag{8}$$

$$\sigma_u = \sigma_{u2} \qquad N_2 \le N$$

This strength degradation model (Eq. 8) was employed in the present example to model the longitudinal fatigue behavior of the graphite fiber. The necessary parameters for the model are σ_{u1}, σ_{u2}, N_1, and N_2. The values of these parameters, chosen for the Hi-NiC Type-S fiber, are shown in Figure 5. Note that these data were not correlated with experiment, but rather chosen based on the expected trend. Given these required parameters for the fatigue damage models for each phase in the SiC/SiC composite, macroscopic or composite fatigue life of both unidirectional and [0/90] cross-ply composite laminates can be simulated. Note although creep-fatigue interaction can be incorporated in the above theory, see [37], it is not included in the present calculations as the fatigue load is applied at room-temperature.

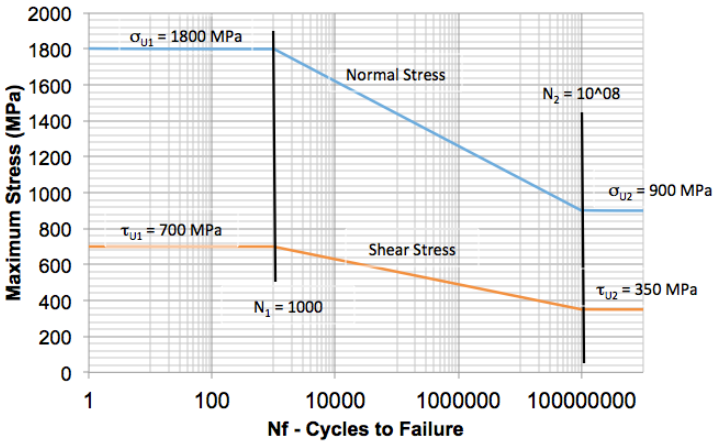

Figure 5 Strength reduction fatigue model parameters assumed for the Hi-NiC Type-S fiber.

4. Results/Discussion

4.1 Residual Stresses

Composite materials usually develop residual stresses because of processing. Advanced CMCs are processed at a high temperature and the composite is cooled down following some time-temperature profile. Since composite constituents can have different coefficients of thermal expansions as well as different creep/relaxation rates, there is a constant stress redistribution (load shedding) from one constituent to another that results in residual stresses developing within the composite in the as-fabricated condition. Residual stresses are important and need to be accounted for as they affect the PLS and UTS of the composite material. In the case of SiC/SiC CMCs, residual stresses arising from the mismatch between the constituents' thermal expansion coefficients are minimal, as both the fiber and matrix are silicon carbide-based constituents. However, there is

usually enough free silicon (Si) within the matrix (which goes through a phase change) that gives rise to residual stresses in the fiber and matrix due to processing. This is particularly true in the MI SiC/SiC composites being analyzed herein. A previous method employed to include such residual stresses in the CMC predictions involved performing separate uncoupled homogenization between free silicon and SiC matrix to get an effective recrystallization strain. An equivalent recrystallization coefficient (CXE) for the homogenized matrix was computed and artificially adjusted to match the composite stress-strain curves and to account for any relaxation that takes place during the processing of the composite. However, the value chosen of the CXE is arbitrary [38]. This approach is fine for a purely elastic analyses as it merely requires knocking down (adjusting) the recrystallization strain to get more realistic residual stresses. However, time-dependent effects or interactions between the free silicon and SiC are missing. Thus, any time-dependent effect, such as temperature rate changes or any post-processing heat treatment preformed on the composite, that will change the residual stresses cannot really be accounted for. Consequently, an alternate approach used herein is to assume a process history, account for the stresses resulting from the phase change, and account for the creep/relaxation of the constituents with time, temperature, and stress. This process explicitly computes the residual stresses resulting from applying this process history while considering the creep/relaxation in various constituents. This approach can also account for any heat treatment that may be performed as a post-processing step.

To demonstrate this approach using NASA's MAC/GMC computer code, a sample processing history along with a heat treatment performed after the processing but prior to any application of mechanical load is shown schematically in Figure 6. A simple power law for the creep/relaxation of the form $\varepsilon' = A\sigma^n$ available in MAC/GMC is used. Constituent properties as a function of temperature as well as parameters for power-law creep are shown in Table 2. Figure 7 shows the qualitative effect on the [0/90] laminate baseline case room-temperature tensile response. The inclusion of residual stresses or any subsequent heat treatment and its effect on residual stress does not change the initial elastic modulus but does influence the predicted PLS as well as the UTS. When the residual stresses are included, the PLS increases and the UTS is reduced (due to pre-straining of the fiber). As mentioned before, since PLS is the upper limit of allowable CMC stress, increasing the PLS of the composite has a beneficial effect in that the allowable stresses on the composite increase. When a heat treatment is performed after the processing but prior to any application of mechanical loads, the PLS decreases and the UTS increases as shown in Figure 7. The exact magnitude of change is dependent upon dwell time at temperature, e.g., dwell of 10000 hrs. at 1100°C shows greater decrease (see purple line, Figure 7) in PLS than does 100 hours (green line). Consequently, the micromechanics analyses performed using MAC/GMC can account for any time related effects on the composite response.

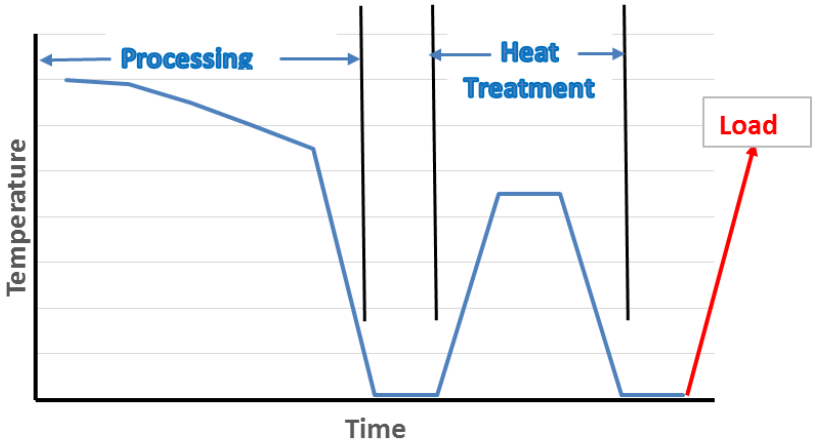

Figure 6 A schematic of a processing history and a subsequent heat treatment applied prior to an application of a mechanical load.

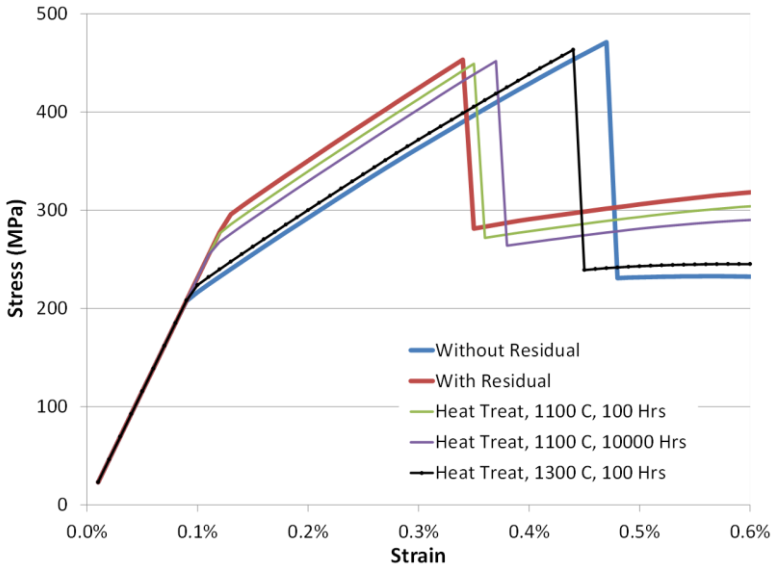

Figure 7 Qualitative effects of heat treatment on [0/90] laminate room-temperature tensile response.

4.2 RUC-Based Modeling in the Presence of Random Microstructures

In a previous paper [22], the statistical influence of microstructure (both ordered and disordered) on the unidirectional and laminated composite effective properties and fatigue life for a graphite/epoxy polymer matrix composite with strong interface was investigated. It was determined that accounting for spatial variations in composite microstructure enables one to simulate observed statistical variations in both effective properties and fatigue life. However, the more computationally efficient GMC is significantly less sensitive to microstructure variations than is HFGMC. GMC typically predicted lower effective properties and higher fatigue lives than did HFGMC for ordered microstructures. Fatigue lives for RUCs representing ordered microstructures with GMC were also higher and significantly outside the range of those lives computed for RUCs with disordered microstructures; whereas fatigue lives predicted with ordered RUCs using HFGMC were within the range of those lives determined using disordered microstructures. Further,

although fatigue lives predicted by HFGMC vary significantly based on individual microstructures (whereas GMC is relatively insensitive), the mean life value (i.e., averaged over multiple microstructure realizations) for a given RUC discretization between HFGMC and GMC was shown to be relatively small (<30%) compared to lives produced using an ordered (single fiber with periodic boundary conditions) microstructure. Note that the actual percentage discrepancy, in the case of disordered microstructures, is highly dependent upon volume fraction and property mismatch between constituents.

In this paper, we again examine the influence of micromechanics idealization (GMC and HFGMC), for both ordered and disordered microstructures, on the unidirectional and laminated composite effective properties, PLS and fatigue life, but this time for a ceramic matrix composite (CMC) with an explicit weak interface. The fiber and interface volume fractions being held fixed at 28% and 13%, respectively and the constituent properties are assumed to be deterministic throughout this study. To evaluate the influence of microstructural variation only, residual stresses are not included in this part of the work.

4.3 GMC and HFGMC RUC and Subcell Refinement: Ordered Microstructures

The various ordered RUCs considered are shown in Figure 8. Figure 9 illustrates the influence of subcell and RUC refinement on the effective tensile and shear moduli, PLS, and fatigue life for four different circular fiber RUCs; RUC-D, -E, -F and -Base shown in Figure 8. Clearly, no subcell discretization dependence is observed for GMC, provided the RUC remains fixed (see RUC-D, -E, -F in Figure 8), irrespective of response parameter examined. It should be mentioned that finite element analyses show mesh dependency. GMC has no mesh dependency because of the assumptions used in the theory i.e., decoupling of normal and shear stresses. However, if the circular fiber representation changes (e.g., RUC-D versus RUC-Base) then both deformation and life (to a greater extent) response are affected. HFGMC does exhibit subcell discretization and aspect ratio dependence (due to coupling of normal and shear stresses) wherein one sees that the transverse normal and transverse shear modulus and PLS are slightly impacted; while the transverse fatigue life at room-temperature (Figure 9d), is significantly affected as it depends more heavily on the accuracy of the local fields. This is expected since GMC is a first order theory (so that fiber volume fraction of a given constituent per row or column in an RUC matter [12]), whereas HFGMC is a second order theory that enables normal shear coupling, see [23]. If the fatigue analysis were to be performed at high temperature, then the fatigue-creep interaction must be accounted for in a manner described in Ref. [37].

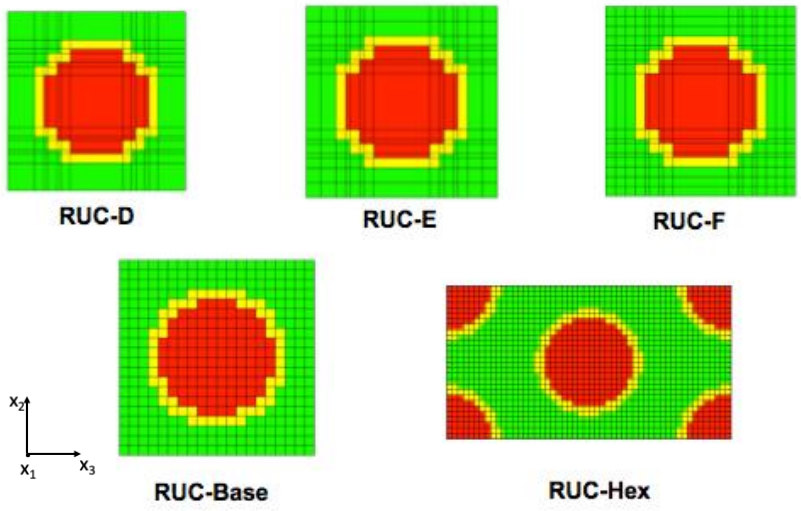

Figure 8 Ordered Repeating Unit Cells where for the square packed architectures matrix discretization is the difference between RUC-D, -E, and –F, i.e., 2, 4 and 6 subcells between fibers, respectively, while RUC-Base has a uniform subcell discretization (i.e., subcell aspect ratio of one).

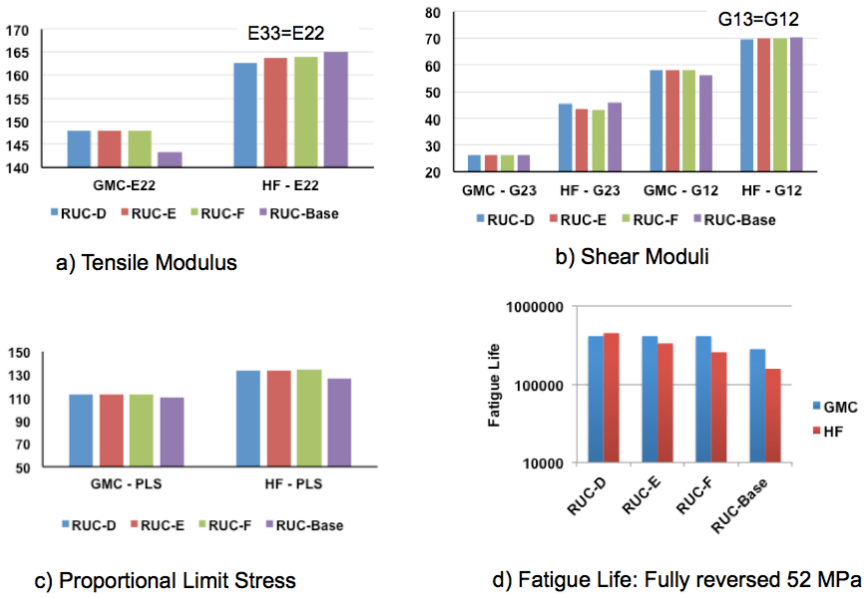

Figure 9 Influence of Subcell Refinement, given circular fiber RUC, on the effective property, PLS and fatigue life (σ_{max} = 52 MPa, R = -1) predicted by GMC and HFGMC.

Comparing the difference between effective composite properties predicted by HFGMC and GMC (typically under predicting), one sees approximately a 13% difference in transverse normal stiffness, 20% in longitudinal shear and 40% difference in transverse shear modulus. GMC typically predicted longer lives than did HFGMC for a corresponding RUC idealization; the difference being almost a factor of 2 for the RUC-Base. Similarly, we see that the fatigue life computed by HFGMC for RUC-Base is approximately half that of RUC-E. Note, although HFGMC is considered more

accurate than GMC, on average it is orders of magnitudes slower than GMC. Therefore, in large structural problems it is important to balance computational efficiency with fidelity (accuracy), particularly in the case of fatigue life calculations.

Figure 10 illustrates the difference in effective tensile and shear moduli, PLS, and fatigue life between two ordered microstructures; a square packed (RUC-Base) and hexagonal packed (RUC-Hex, see Figure 8) fiber architecture. Comparing the difference between hexagonal packed effective composite properties predicted by HFGMC and GMC (typically under predicting), one sees approximately a 17% difference in transverse normal stiffness (note for GMC $E_{33} \neq E_{22}$ for RUC-Hex), 30% in longitudinal shear (note for GMC $G_{13} \neq G_{12}$ for RUC-Hex), and 50% difference in transverse shear modulus, see [16] for more details. In case of failure the difference in hexagonal packing between methods is significantly greater than for square, with the PLS being approximately 30% and fatigue life 600%. It is interesting to note that the difference between packing arrangements for GMC is significantly more than it is for HFGMC due to the presence of the weak interface and lack of normal-shear coupling that is inherent to GMC micromechanics. Finally in Figure 11 stress level versus fatigue life cycles (S-N curves) for a unidirectional laminate loaded transverse to fibers, i.e., [90] and a symmetric cross-ply laminate, [0/90]s, are shown, given these two different packing arrangements. Most notable is the significant variation in both packing and method for the [90] laminate as compared to the [0/90]s. This clearly illustrates that microstructure variation is significantly reduced by the presence of [0] plies within the laminate since longitudinal (fiber direction) response is predominately influenced by the fiber behavior. Furthermore, differences between micromechanics methods are also minimized when predicting laminates containing zero plies, see [23] for a detailed discussion of progressive damage under static loading.

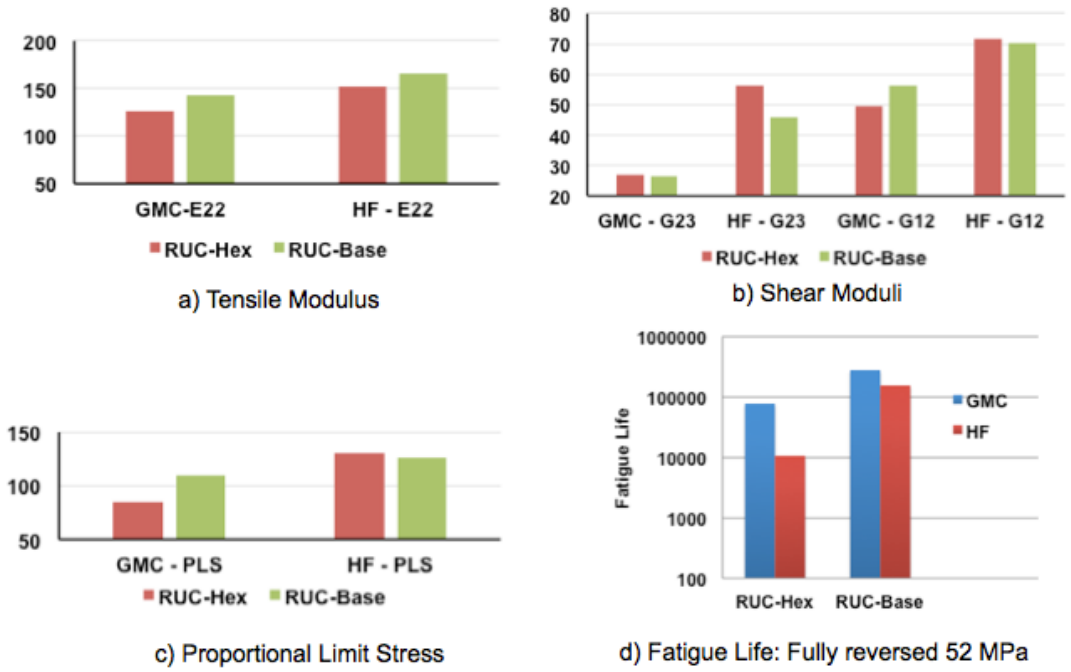

Figure 10 Influence of ordered fiber packing arrangements; Hexagonal vs. Square (see Figure 7).

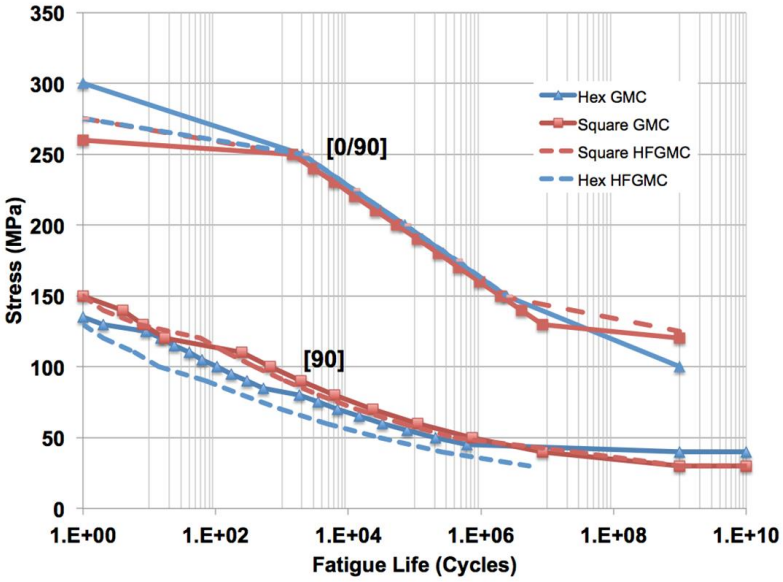

Figure 11 S-N curves for two ordered microstructures containing: square and hexagonal fiber packing architecture.

4.4 Ordered Versus Disordered Microstructure

Realistic composite microstructures typically are not well ordered, particularly in the case of CMCs, which have lower fiber volume fractions of less than 35% and thus more opportunity for fiber movement. Consequently, it is important to understand the influence of random fiber placement (disordered microstructure) on the deformation (effective properties, PLS) and failure (e.g., fatigue life) behavior of the composite. Given the above results, the 20 × 20 RUC-Base (see Figure 8) was selected as our fundamental building block for generating an RUC containing more than a single fiber. Multiple fiber RUC studies containing 4, 25 and 100 fibers in an RUC were conducted to evaluate the effects of random fiber distributions as well as to decide how many fibers one should use in an RUC with random microstructure and yet maintain a proper balance between efficiency (CPU time) and accuracy (some measure of error). RUCs with random fiber placement were generated using a RUC generator [38]. Figure 12 shows average values of in-plane transverse modulus, E_{22} and in-plane shear modulus, G_{12} for a [90] laminate as a function of number of fibers in the RUC using HFGMC micromechanics analyses using random fiber placement. Results are based on 100 simulations for each case. Properties are normalized by the average values of HFGMC analyses with an RUC containing 100 fibers. It also shows normalized computational time normalized by the CPU time required for a HFGMC analysis for a square pack RUC (0.127 sec). For comparison, CPU time taken for a regular Hex pack HFGMC analysis is 0.51 sec. on a standard stand-alone PC. Results show that when you change the random RUC from 4 to 9 fibers, the computational cost increases by approximately three times while the improvement in accuracy is less than 2%. For RUCs containing 16, or more fibers, the computational costs increase exponentially. Based on these observations, it was decided to utilize a 40 × 40 four fiber RUC consisting of a total number of 1600 subcells as our baseline multi-fiber RUC to study the effects of random fiber distribution. Ten samples of four-fiber RUCs out of the 100 randomly generated and analyzed instances are shown in Figure 13. The nominal fiber and BN coating volume fractions are 28% and 13%, respectively. Constituent material properties remain the same as given in Table 1.

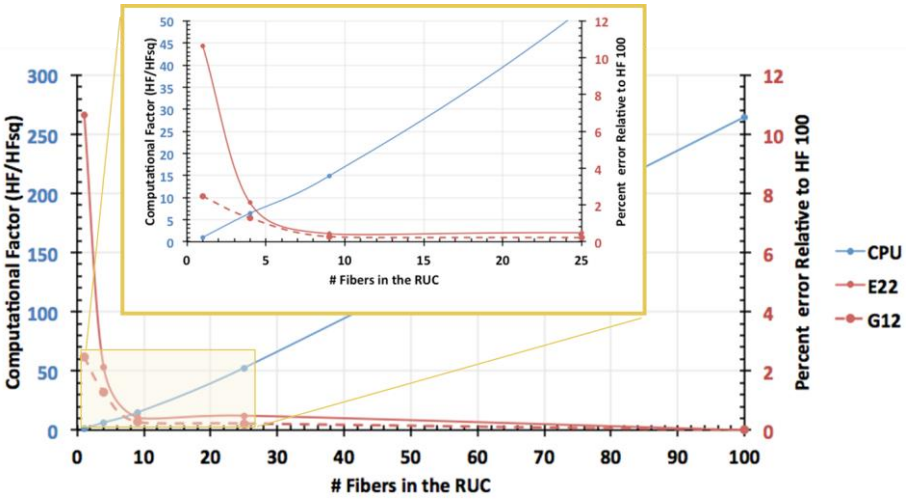

Figure 12 HFGMC results for a [90] laminate for average values of transverse modulus and in-plane shear modulus as well as the normalized computational cost. Results are based on 100 simulations for each case.

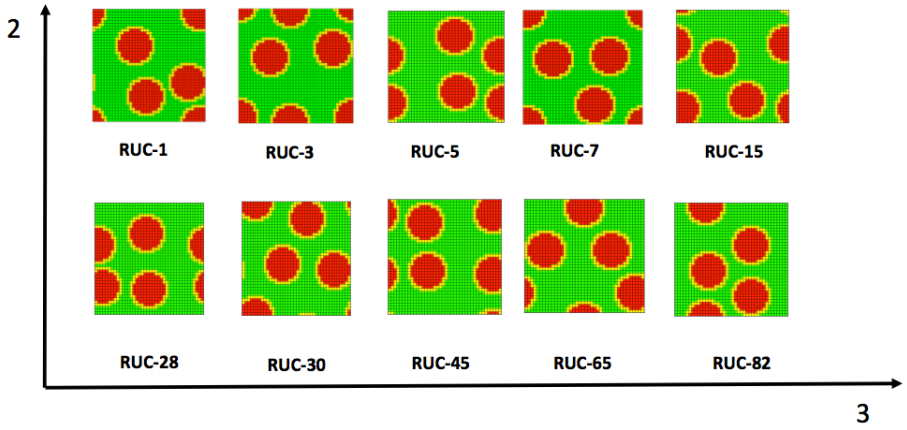

Figure 13 A sampling of the 100 randomly generated disordered RUC microstructure with four circular fibers within.

Two types of laminates will be examined, unidirectional [90], and cross-ply $[0/90]_s$. Although unidirectional laminates loaded transverse to the fiber direction, i.e., [90], are not employed in practice, this type of laminate will exhibit the greatest sensitivity to microstructural influences and is often the most examined in the literature. Cross-ply laminates are more relevant for practical usage. It should be noted that in a longitudinal [0] composite (i.e., loaded along the fiber direction) the microstructure has minimal to no influence on the response/properties of such a composite. The properties and response in that situation generally depends only upon the volume fractions of each constituent as well as the properties of the constituents themselves. Effective moduli, PLS and fatigue life results, in terms of mean, standard deviation (St. Dev.), range and coefficient of variation (C.O.V.), for all 100 instances simulated by GMC and HFGMC for [90] and $[0/90]_s$ laminates are tabulated in Table 3 and Table 4, respectively. Also results for square and hexagonally packed, ordered, microstructures are given for each laminate as well.

Table 3 [90] SIC/SIC laminate; 100 simulations; 4 circular fibers.

	In-Plane Modulus, Ex (GPa)		**In-plane Shear Modulus,Gxy (GPa)**		**Prop. Limit Stress, PLS* (MPa)**		**Fatigue Life (60 MPa; R = -1)**	
	GMC	**HFGMC**	**GMC**	**HFGMC**	**GMC**	**HFGMC**	**GMC**	**HFGMC**
Mean Value	101.2	152.4	39.2	69.5	59.3	95.5	4,752	6,673
St. Dev.	13.3	6.3	5.5	1.2	21.8	13.9	10,915	7,024
Range	82.5-136	139.7-164.1	31.6-53.4	66.3-72.2	38.1-105	73.3-124.8	0-73,328	23-37,983
C.O.V.	13.20%	4.10%	14%	1.70%	36.80%	14.60%	229.68%	105.26%
Sq. Pack	143.4	165	56.2	70.3	110	186.8	111,501	63,771
Hex Pack	126.1	152.7	49.5	71.4	52.7	133	32,466	4,666

Table 4 $[0/90]_S$ SIC/SIC laminate; 100 simulations; 4 circular fibers.

	In-Plane Modulus, Ex (GPa)		**In-plane Shear Modulus, Gxy (GPa)**		**Prop. Limit Stress, PLS* (MPa)**		**Fatigue Life (150 MPa; R = -1)**	
	GMC	**HFGMC**	**GMC**	**HFGMC**	**GMC**	**HFGMC**	**GMC**	**HFGMC**
Mean Value	202.4	227.8	39.2	69.5	149	176.7	1,986,456	2,063,349
St. Dev.	6.7	3.1	5.5	1.2	46.2	20.7	10,384	18,417
Range	193-219.7	221.5-233.6	31.6-53.4	66.3-72.2	94.3-239	145.2-233.4	2,034,392-1,9781,110	2,093,137-2,032,599
C.O.V.	3.30%	1.40%	14%	1.70%	31%	11.70%	0.52%	0.89%
Sq. Pack	223.4	234	56.2	70.3	182.6	211.2	1,983,623	2,000,196
Hex Pack	215.5	228.7	49.5	71.4	227.9	224.2	2,453,355	2,461,295

In general, there is a significant difference between the GMC and HFGMC simulated properties (effective moduli and PLS) as well as fatigue life when dealing with disordered microstructures. This is mainly due to the lack of normal and shear stress coupling within GMC, which is exacerbated by the presence of the weak interface coating around each fiber. Comparing Table 3 and Table 4 results, it is apparent that the C.O.V is significantly reduced for the cross-ply laminate (with generalization to any fiber dominate laminates, i.e., with [0] plies present) as compared to the [90] laminate for the in-plane transverse modulus and fatigue life, whereas in the case of the in-plane shear modulus and PLS the C.O.V are very similar. This is reasonable since the in-plane shear modulus is controlled by the fiber properties and fiber volume fraction and the PLS is controlled by the "first ply failure" which in these two laminates corresponds to the [90] ply as [90] ply fails first in a cross-ply laminate. It is interesting to note that the C.O.V in fatigue life for the $[0/90]_s$ laminate is less than 1% since it is dominated by the cyclic dependent fiber strength which provides significantly longer cyclic life (at least two orders of magnitude) than the cyclic life of the matrix at the given fully-reversed applied load level of 150 MPa (see Figures 4 and 5). Finally, assuming that HFGMC predictions are accurate, it also appears, as expected, that results predicted using an ordered hexagonal packed microstructure agree reasonably well with the HFGMC mean value predictions coming from 100 instances of disordered microstructures for both [90] and $[0/90]_s$ laminates. The only exception appears to be in the case of in-plane shear modulus, PLS and fatigue life for the [90] and $[0/90]_s$ laminates where square packing agrees better.

Figures 14 and 15 show the monotonic stress-strain response for the upper and lower bound disordered instances as well as the square (square symbol) and hexagonal (triangular symbol) ordered microstructure RUCs for the [90] and $[0/90]_s$ laminates, respectively. In both figures, GMC and HFGMC predictions are made using the upper and lower bound RUC instances computed associated with GMC (dashed lines) and HFGMC (solid lines) bounds. Again the variation between the upper and lower bound is significantly greater in the [90] case (Figure 14) as compared with the $[0/90]_s$ laminate case (Figure 15). For both laminates, HFGMC predictions (purple) are the highest when using the upper bound instances obtained from either GMC (RUC-45) or HFGMC (RUC-28). Similarly, GMC predictions (black) are the lowest when using the lower bound instances obtained from either GMC (RUC-15) or HFGMC (RUC-28).

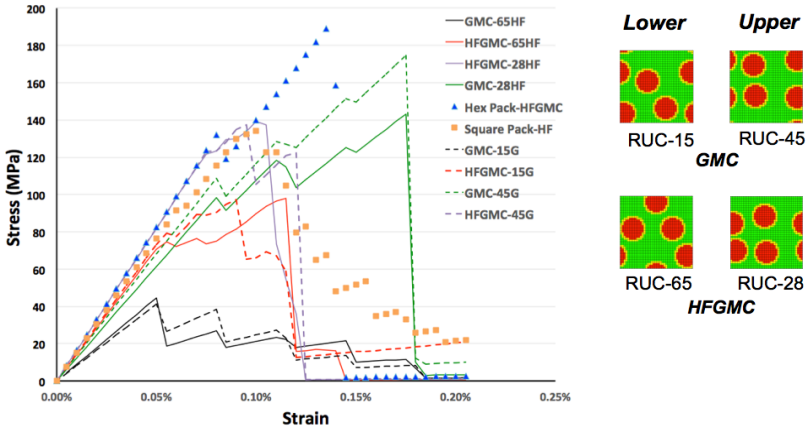

Figure 14 SiC/SiC [90] laminate stress-strain responses simulated using GMC and HFGMC for the upper and lower bound disordered architectures as well as square and hexagonal ordered architectures.

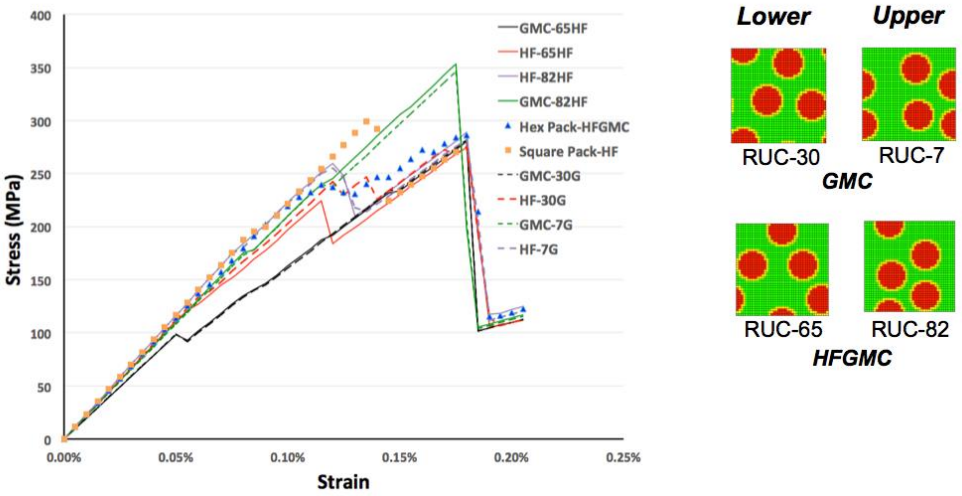

Figure 15 SiC/SiC [0/90]s laminate stress-strain responses simulated using GMC and HFGMC for the upper and lower bound disordered architectures as well as square and hexagonal ordered architectures.

The influence of microstructure on fatigue life is seen clearly in the fatigue life versus instance scatter plots for [90] and $[0/90]_s$ laminates shown in Figures 16 and 17, respectively. For the [90] layup, see Figure 16, although the predicted fatigue life can vary significantly between GMC and HFGMC for a given instance, the mean values between the two methods only differ by approximately 28.7%. Table 3 indicates that the C.O.V. for fatigue given by GMC is approximately 230% while for HFGMC it is 105%. In the case of $[0/90]_s$ layups, see Figure 17 – note here the fatigue life is normalized by HFGMC mean value (2,063,349), the difference in predicted fatigue life for any instance between GMC and HFGMC is less than 8% while the difference in mean lives is also approximately 3.7%. Table 4 indicates that the C.O.V. for fatigue given by GMC is approximately 0.5% while for HFGMC it is 0.89%. Clearly, the [0] ply suppress the microstructure variation observed in a [90] ply (see Figure 16) such that the significantly more computationally efficient GMC method (although not well suited for accurately predicting unidirectional composite disordered microstructures) can be employed efficiently with very good accuracy for $[0/90]_s$ laminates. Note the average computational time for the 100 instances for HFGMC was 1600 seconds while GMC was only 6 seconds: a 266 times improvement. We believe this conclusion should be extendable to other layups containing [0] plies as well. This will be confirmed in future studies.

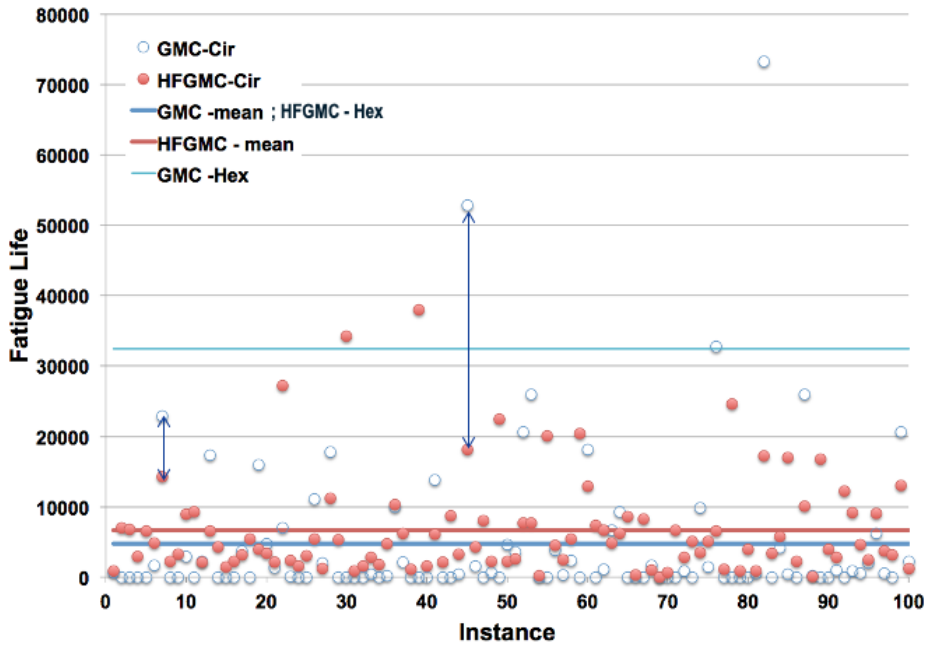

Figure 16 SiC/SiC [90] laminate, v_f = 0.28, fatigue life simulated using GMC and HFGMC for 100 random disordered microstructure instances. Loading is uniaxial 60 MPa fully reversed cyclic loading, and applied transverse to the fiber direction. Four fibers are contained within each RUC.

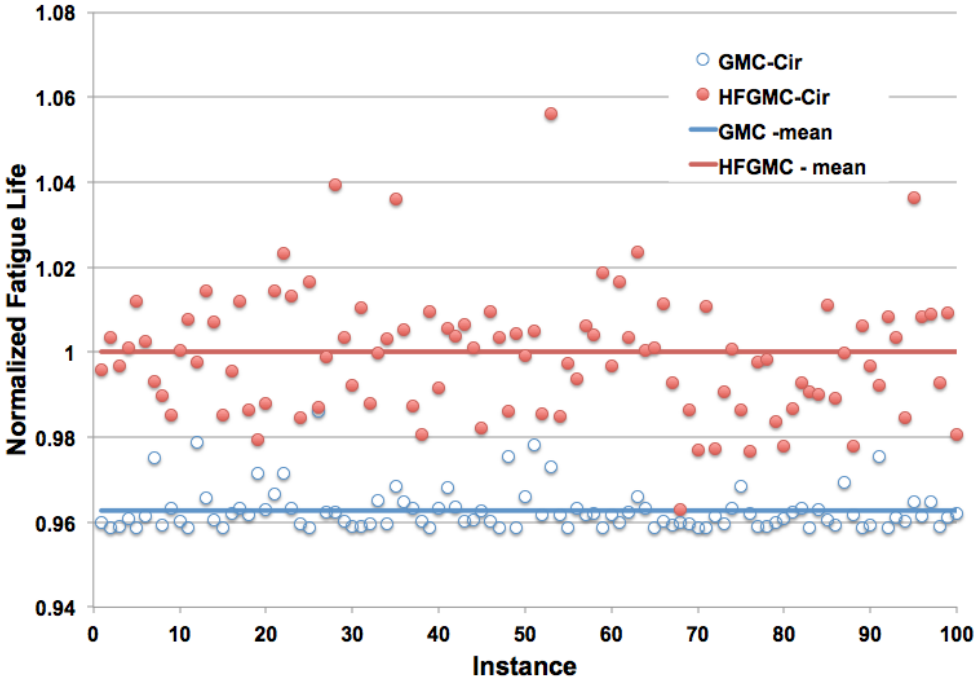

Figure 17 SiC/SiC [0/90] laminate fatigue life simulated using GMC and HFGMC for 100 random disordered microstructure instances subjected to a uniaxial 150 MPa, fully reversed cyclic applied load. Four fibers are contained within each RUC. Normalization factor is 2,063,349.

Figure 18 (a) illustrates multiple S-N curves associated with the minimum (brown line with star), average (red dashed line), and maximum (brown with diamond symbol) lives of 100 random RUCs for a [90] laminate. In addition, a hexagonal packed periodic microstructure RUC (blue line) is also provided in Figure 18. Clearly, this hexagonal RUC matches the mean of 100 runs at higher load levels but as the load decreases the hexagonal RUC provides significantly shorter lives. Consequently, the hexagonal RUC is conservative for all load levels. Also, apparently above 55 MPa the failure mechanism changes from matrix fatigue damage to interface failure. Note this is clear from comparing RUC-69 (minimum response at 60 MPa) and RUC-39 (maximum response at 60 MPa). Yet these responses switch at 55 MPa and below. There is a change in failure mechanism – interface failure dominates at higher applied stresses, while matrix cracking at lower applied stresses. Figure 18(b) shows the S-N curve for a [0/90] laminate and the scatter in these curves is significantly less than what is observed for a [90] laminate. As mentioned before, the presence of [0] plies in a laminate suppresses the scatter that arises due to microstructure variation.

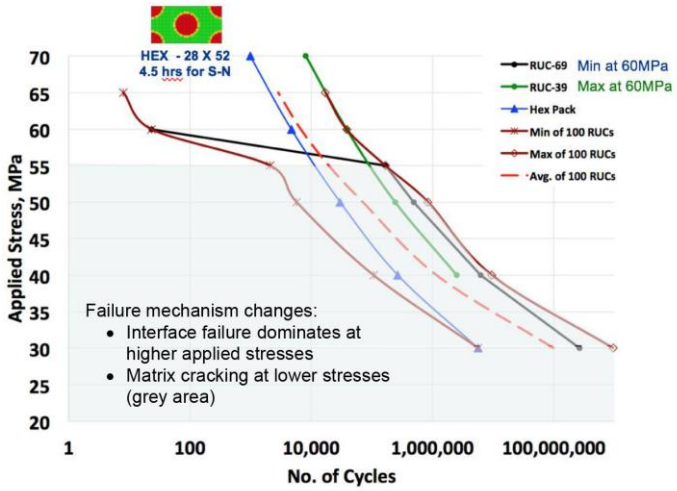

(a) [90] laminate; denotes a change in failure mechanism – interface failure dominates at higher applied stresses while matrix cracking at lower applied stresses (grey area)

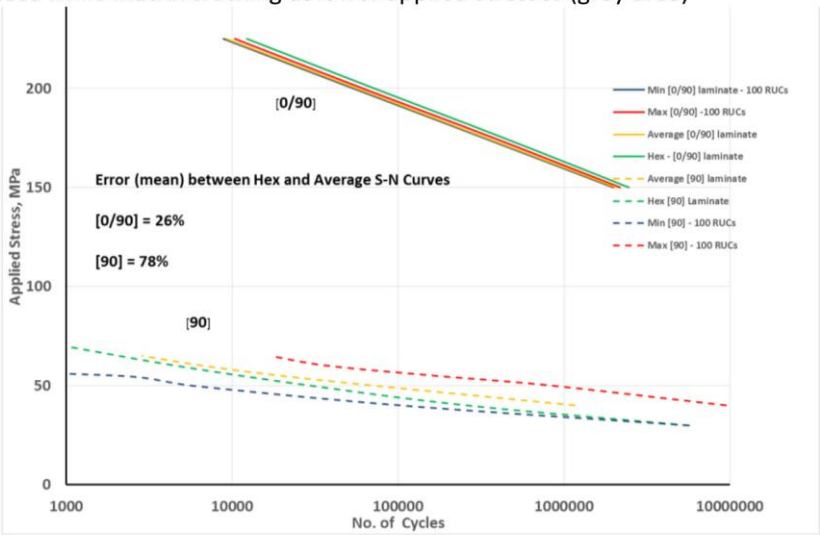

(b) [0/90] Laminate, Range of [90] laminate also plotted for comparison

Figure 18 Fatigue S-N Curve for SiC/SiC (a) [90] laminate and (b) [0/90] laminate; v_f = 0.28, simulated using HFGMC for 100 random disordered microstructure instances.

Figure 19 illustrates the resulting probability density functions given 4 random fibers (noted as 2 × 2), 9 random fiber (denoted as 3 × 3) and 25 random fiber (denoted as 5 × 5) RUCs loaded uni-axially at 50 MPa. All simulations are conducted using HFGMC micromechanics method and indicate that the three resulting PDF responses are non-normal distributions. No residual stresses were included in these analyses. Note that as the number of fibers is increased in each RUC the amount of scatter reduces and the mean response approach the mode. The resulting non-normal distribution suggest that when performing design or computing design allowables, the mode should be used over that of the mean response since it represents the more prevalent life as opposed to usual A or B basis type of calculations that inherently assume a normal distribution of the property of interest. Also, on average the mode life is approximately 58% more conservative than the associated mean life. Lastly, the hexagonal pack RUC (from Figure 8) is shown to match the mode of the 4 fiber RUC and over predict the mode of the 9 fiber RUC distribution by a factor of 3.75. However, a significant speed up 18× and 100× over random RUCs is observed. Note the mean and mode of the fatigue life distribution are even shorter for 25 fiber RUCs, see Figure 19. Additionally, although not shown a coarser hexagonal pack RUC (14 × 26) was shown to predict a longer life (i.e., 4.6×) than that of the finer (28 × 52) hex pack RUC yet at a significantly faster (14×) computational speed. Finally, from these results it appears that an ordered HEX RUC provides a good balance between efficiency and fidelity for multiscale modeling. Also, random microstructure variation is significantly reduced when one considers laminated composites where certain percentage of the plies are oriented in the [0] or along the primary loading direction.

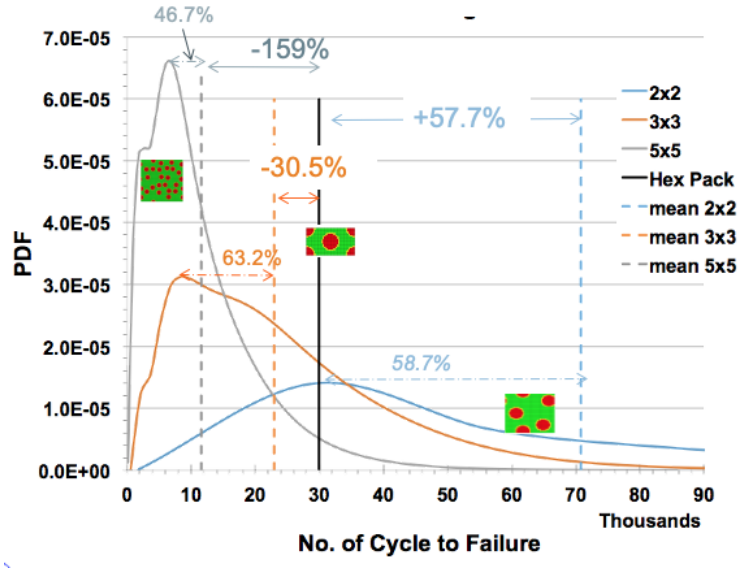

Figure 19 Simulated fatigue life probability distribution function for a SiC/SiC [90] laminate, v_f = 0.28, using HFGMC for 100 random disordered microstructure instances given 4, 9 and 25 fibers in an RUC subjected to an applied stress of 50 MPa (see Figure 18a).

4.5 Manufacturing Variability: Variable Fiber Diameter/Coating Thickness

The previous section dealt with a single aspect of microstructure variations, fiber center location. Here, in addition to fiber center location variability, variability involving fiber diameter and interface

coating thickness will be examined. The primary question to be addressed is whether there is any advantage (relative to moving the mean composite response) in trying to hold the fiber diameter and/or coating thickness constant. This is a practically significant manufacturing question since it is technologically possible (but requires significant resource investment) to achieve uniform fiber diameter and/or fiber coating thickness. Although, this is a very difficult if not intractable problem to examine experimentally due to the difficulty in controlling the various sensitive parameters (i.e., fiber volume fraction, fiber diameter, coating thickness, etc.) throughout the domain over which the response is being averaged. However, micromechanics enables one to easily control these parameters and assess their sensitivity and influence on the composite response. Therefore, the question is, is it a worthwhile investment of resource?

To answer this, four sets of 100 random disordered microstructures (idealized with four square shape fibers to aid in the automatic generation of the corresponding RUCs) were simulated using a random RUC generator [39]. Every instance had the same overall fiber volume (28%) and interface volume (13%) fractions maintained. In this way the effect of volume fraction was eliminated from the study results, which most likely would be extremely difficult to achieve experimentally. Figure 20 illustrates a sampling of twelve RUCs with three RUCs from each set of 100: top row is the baseline (fixed fiber/fixed coating), second (variable fiber/fixed coating thickness), third (fixed fiber/variable coating thickness) and fourth or bottom row (variable fiber and variable coating thickness). Each row provides the microstructure associated with the lowest (LOW), the mean (AVG), and the highest (HIGH) PLS for the given conditions. Note, the range in variations in fiber diameter and coating thickness was taken to be 9.6 to 14.4 microns and 1.28 to 1.9 microns, respectively. This was equivalent to a C.O.V. of 0.2 assuming a uniform distribution from the baseline of 12-micron fiber diameter and 1.26-micron coating thickness. Table 5 and Table 6 show the statistical results (mean, standard deviation, range, and coefficient of variation) for the elastic properties (transverse and shear modulus), PLS and ultimate strength for all four types of simulations given a unidirectional, [90], and cross-ply, [0/90]s laminate, respectively. Based on the [90] results and due to the additional computational time required to conduct cross-ply laminate cases, only the baseline and fourth-variable fiber/variable coating thickness simulations were done for the $[0/90]_s$ laminate case and shown in Table 6.

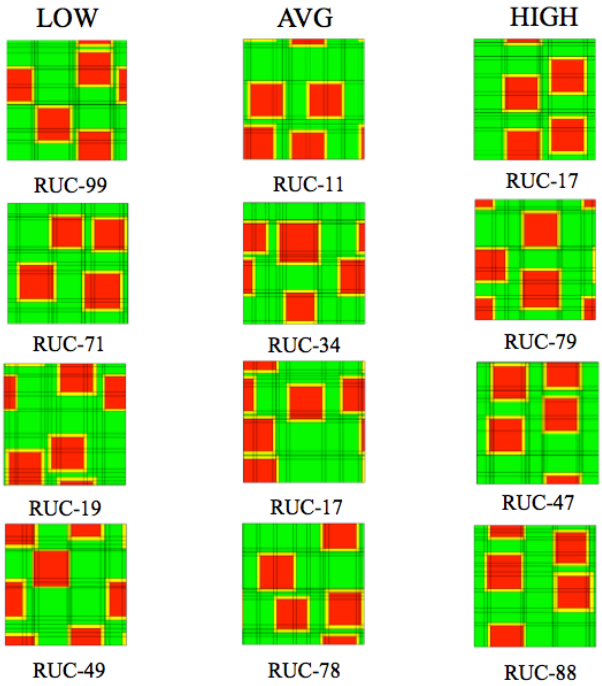

Figure 20 A sampling of the 100 randomly generated disordered RUC microstructure with four square fibers within; First row - constant fiber diameter and coating thickness, Second row - variable fiber diameter and constant coating thickness, Third row - variable coating thickness and constant fiber diameter, and Fourth row – variable fiber diameter and variable coating thickness. All volume fractions held constant.

Table 5 [90] Sic/Sic laminate; 100 simulations; 4 square fibers in the RUC.

	Transverse Modulus, E2 (GPa)				Axilal Shear Modulus, G12 (GPa)			
	Baseline	**Variable D**	**Variable Interface t**	**Variable D & Interface t**	**Baseline**	**Variable D**	**Variable Interface t**	**Variable D & Interface t**
Mean Value	151.7	151.2	152.4	152.6	66.7	66.5	66.9	67.0
St. Dev.	9.6	9.8	9.0	9.9	2.4	2.6	2.2	2.6
Range	133.0-168.6	132.0-172.0	131.3-169.6	131.5-172.2	59.1-72.3	56.7-71.2	58.8-71.7	59.5-73.6
C.O.V.	6.3%	6.5%	5.9%	6.5%	3.5%	3.9%	3.3%	3.9%
	Transverse Prop. Limit Stress, PLS* (MPa)				**Transverse Ultimate Stress (MPa)**			
	Baseline	**Variable D**	**Variable Interface t**	**Variable D & Interface t**	**Baseline**	**Variable D**	**Variable Interface t**	**Variable D & Interface t**
Mean Value	91.7	90.1	89.2	90.4	106.9	105.5	106.9	107.5
St. Dev.	31.4	16.2	16.7	18.4	31.4	29.8	30.0	31.2
Range	62.8-138.7	64.1-131.85	60.6-138.0	46.9-132.8	64.8-184.7	66.6-202.8	67.7-186.8	57.2-183.1
C.O.V.	20.2%	18.0%	18.7%	20.4%	29.3%	28.2%	28.1%	29.0%

Table 6 $[0/90]_s$ Sic/Sic laminate; 100 simulations; 4 square fibers in the RUC.

	In-Plane Modulus, Ex (GPa)		In-Plane Shear Modulus, Gxy (GPa)		In-Plane Prop. Limit Stress, PLS* (MPa)		In-Plane Ultimate Stress (MPa)	
	Baseline	**Variable D & Interface t**	**Baseline**	**Variable D & Interface t**	**Baseline**	**Variable D & Interface t**	**Baseline**	**Variable D & Interface t**
Mean Value	227.6	228	66.8	67	287.3	155.3	287.3	289.5
St. Dev.	4.7	4.9	2.3	2.6	15.6	25.2	15.6	18.7
Range	218.7-235.9	218.0-237.6	59.4-72.3	59.4-73.7	113.6-230.0	110.5-222.2	269.4-340.2	270.5-341.8
C.O.V.	0.021	0.021	0.035	0.039	0.171	0.162	0.054	0.065

Clearly in the case of transverse loading of unidirectional composite or a [90] ply, little change is observable (see Table 5) in the normal and shear modulus values while strength values show significant variation. As expected, any observed variation is reduced when laminates containing zero plies are considered, see Table 6. Consequently, it appears that devoting any resources to reduce the variability in fiber diameter and/or coating thickness would be unprofitable since it would have minimal impact on shifting the mean of a given static property. Rather, resources should be expended to ensure the desired volume fraction of a given constituent is obtained, since this will shift the mean significantly.

It should be noted that in all microstructural aspects examined the influence of residual stresses due to processing have been ignored. Consequently, the above conclusion may not persist with the inclusion of residual stresses, since microstructural features should strongly influence these local residual stresses, which in turn will impact local failure and thus the PLS and UTS predictions.

4.6 Multiscale Modeling of Test Coupons

Multiscale analyses described here were performed using NASA's FEAMAC computer code. FEAMAC software couples ABAQUS/Standard commercial finite element software package with MAC/GMC micromechanics software for performing multiscale analyses all the way from the constituent to structural scale. In the FEAMAC computer code, ABAQUS calls MAC/GMC to determine the material response at the integration points within each element(s) or groups of elements identified within the structural finite element analysis (FEA) model. Any damage or failure is checked at the local level and material stiffnesses are adjusted accordingly. Updated homogenized material constituent properties are then passed on to the structural analyses during the next increment of global loading. MAC/GMC operates as an evolving non-linear anisotropic constitutive model within ABAQUS, representing the composite as a homogenized heterogeneous material. In performing FEAMAC analyses, the user is always confronted with the question of what size RUC or microstructural architecture should be used when performing these analyses. One would like to include or represent the salient microstructural features described above (to represent the multiphase material) yet still have a practical tool for multiscale analyses. Clearly, since these analyses are quite resource intense, one wants to use as simple an RUC as possible (i.e., one with very few subcells and efficient micromechanics, e.g., GMC, analyses) to maintain a proper balance between efficiency and fidelity. It was reasoned in prior sections that to properly account for realistic disordered microstructures, a HEX RUC with HFGMC analyses would provide us with a statistical median of the response and yet keep the analyses computationally manageable. However, when performing multiscale analyses even an ordered HEX RUC would require significant resources of computing power and CPU time. Additionally, one must keep the length scale of the structural model to length scale of material microstructure in mind when deciding on an appropriate RUC for conducting single or multiscale analyses. Figure 21 shows a finite element mesh of a typical CMC test coupon as well as micrographs of the associated microstructure.

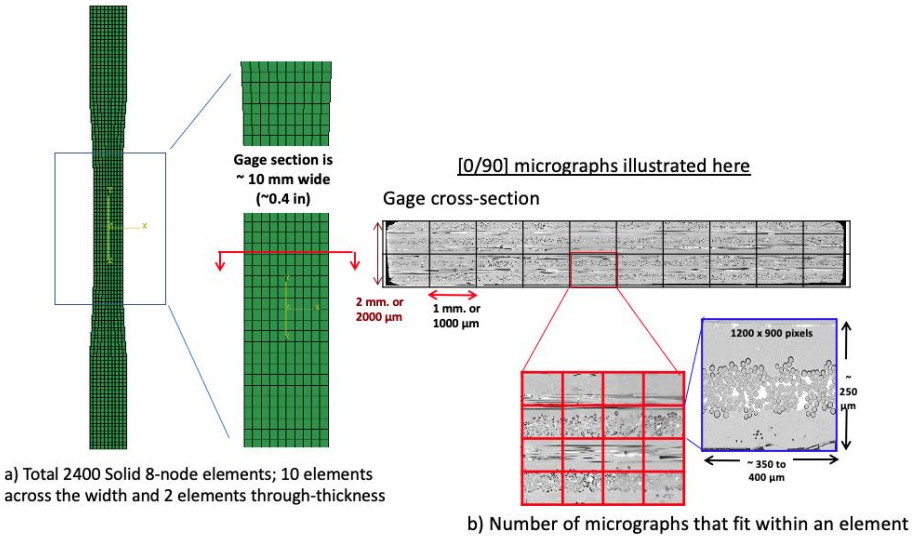

Figure 21 Test specimen (smooth test coupon) showing a comparison of length scales.

As shown in the figure, a typical gage section is 0.4 inches wide (~10 mm) and there are 10 elements across the width of the specimen. Given the size of a typical micrograph and the length of each element as shown, approximately 4 micrographs per ply would fit within each element. It means then, in general, each element's response represents a combination or an average of all the micrographs and their associated features. Thus, one can represent the microstructural features using a simple RUC to represent these features in an average sense. Note the specific RUC representation, be it unidirectional (doubly periodic) or cross-ply (triply periodic), will be intimately linked with the number elements used to describe the through thickness direction of the structure (or in this case specimen). Usually, the test specimens are 8 ply laminates but just to speed up our computations, the model has two elements through-the-thickness for unidirectional [0] laminates using solid 3-D elements and four elements through-the thickness for [0/90]s laminates when using 3-D solid elements. If using continuum shell elements in the model for a cross-ply laminate, there are two elements through-the-thickness, but each element has a 0 and 90 layer when simulating a cross-ply [0/90/90/0] laminate or alternatively, one can use a triply-periodic [0/90] RUC and two elements through-thickness – as shown in the final example. As mentioned before, even using an ordered HEX RUC with HFGMC analyses may not be computationally feasible even for this sized structure.

It is important to maintain idealization consistency in any analysis and specially in a multiscale analysis. Many interdependent factors are comprised within the concept of idealization consistency and can be classified into three main categories: theoretical, mechanistic, and numerical consistencies. Theoretical consistency requires preserving the mathematical aspects (e.g., theory, model dimensionality, functional form, etc.) used throughout characterization to prediction. For example, if the model was characterized using the High Fidelity GMC (HFGMC) theory, which provides more accurate local stress and strain field predictions than standard GMC, the same theory should be used in subsequent predictions as well, since the associated constitutive model parameters where calibrated assuming this theory. Mechanistic consistency would be associated with assumed measures and definitions of damage and modes of failure and their interactions. For example, if matrix damage or delamination is a major mechanism leading to failure of a laminate, it should be accounted for not only in the final prediction but also during characterization. Length

scale (e.g., material volume element) and mesh accuracy are both examples that would fall within the numerical consistency category and thus the preservation of these accuracies from characterization to prediction is important. It is important to remember that these categories are typically not mutually exclusive and thus the influence of one on another is often difficult to explicitly determine. This is particularly true in the case of multiscale analysis wherein all factors can interact aggressively as one traverses various length scales [40].

The unidirectional specimen, shown in Figure 22, was analyzed using a very simple 5x5 doubly periodic RUC (25 subcells) with square fiber packing shown as an insert in Figure 22 and using the GMC method. The results for the stress-strain curve for a [0] composite is shown in Figure 22. The matrix strength is assumed to *vary spatially*, throughout the gage section, to represent the random occurrence of flaws, cracks, voids, and any other irregularity as well as material inhomogeneity. Blue curves represent two simulations of spatially varying matrix strength. These results are compared with a case in which the matrix strength is assumed *spatially constant* so that failure would initiate just outside the gage section where a global stress riser is present. When the matrix strength is assumed to be constant, a sharp drop in the stress strain curve is observed in the simulation, see the green curve in Figure 22. However, the measured data, shown as red curves, does not show such behavior, i.e., the stress-strain curves show a smooth transition. When matrix strength is assumed to be spatially variable, the stress-strain curve (blue line in Figure 22) shows a similar trend to that observed in the measured data. Obviously, one can calibrate the parameters to better match the simulation results with the measured data, but that was not the intent of these analyses. To speed up the analyses, the multiscale computations were performed only in the gage sections (grip areas were excluded from multiscale analyses and an equivalent (effective) anisotropic material property were provided for these elements). Residual stresses due to processing were simulated in these analyses. Run times were approximately 40 minutes per run on a typical Windows desktop computer using a single CPU[1].

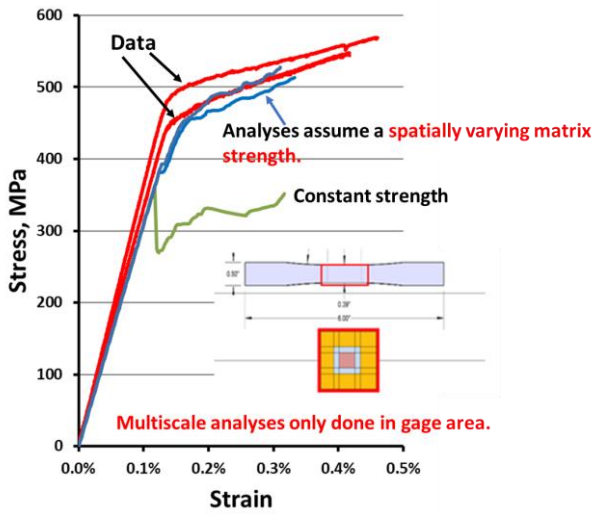

Figure 22 Response of a unidirectional [0] CMC composite coupon, see [1] for data.

[1] A new thread safe multiscale analysis code, known as NASMAT, capable of being used on a High-Performance Computing (HPC) system, is currently under development at NASA GRC. Version 1.0 was released in Nov 2019.

For purely illustrative purposes, straight sided coupons with stress riser features were also analyzed using FEAMAC. For example, a unidirectional [0] CMC composite open hole coupon, a cross-ply $[0/90]_s$ CMC open hole coupon and a unidirectional [0] double-notched coupon were analyzed. The purpose of these analyses is to demonstrate the general capabilities of the FEAMAC computer code in solving multiscale problems. In all these analyses, a multiscale GMC analysis employing a 6x8 RUC using two fibers hexagonally packed, with spatially constant strength were employed in all elements. Also, in all these analyses, residual stresses due to processing were simulated prior to the application of mechanical loading. A process or time-temperature profile as shown in Figure 6 was utilized without any heat treatment.

Figure 23 shows the stress-strain curve and damage initiation/progression for a [0] open hole specimen. The model has 1540 solid 3-D elements with two elements through the thickness. The CPU time for the analysis was approximately 2.7 hours. As shown in the figure and expected [41], damage initiation is localized near the hole, and it progresses outward as one would expect. Here matrix strength was assumed to be constant spatially. The damage state marked at three stress magnitudes is also shown in Figure 23. It should be noted that the damage initiates at the load levels marked 1 and 2 but globally no significant deviation from linearity in the global stress-strain curve is observed.

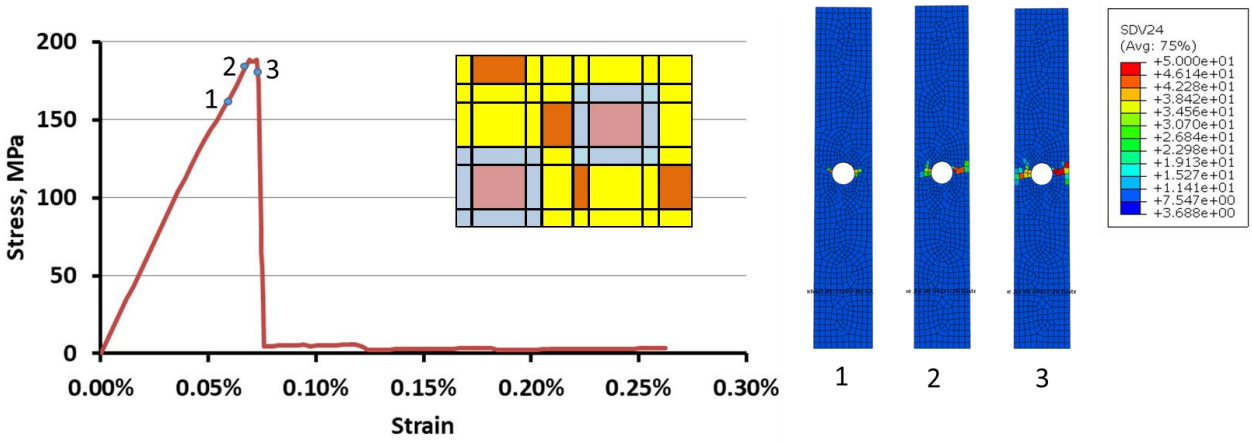

Figure 23 Response of a unidirectional [0] CMC open-hole coupon (hole diameter/specimen width = 0.4); A four-phase 6 × 8 RUC used in the analysis is shown in the inset. SDV24 is a measure of damage in the specimen.

In Figure 24, results associated with an open-hole specimen with a $[0/90]_s$ laminate are shown. This model has 2000 continuum shell elements, wherein 2 elements through the thickness are assumed. Each element has two layers, one representing [0/90] plies and other element representing [90/0] plies. Damage initiation and progression is localized near the hole as expected and shown at the right in Figure 24 at the stress levels marked 1 and 2. The CPU time for this analysis was approximately 4.5 hours and a multiscale analysis (using the RUC shown in the insert with spatially constant matrix strength) was performed for all elements.

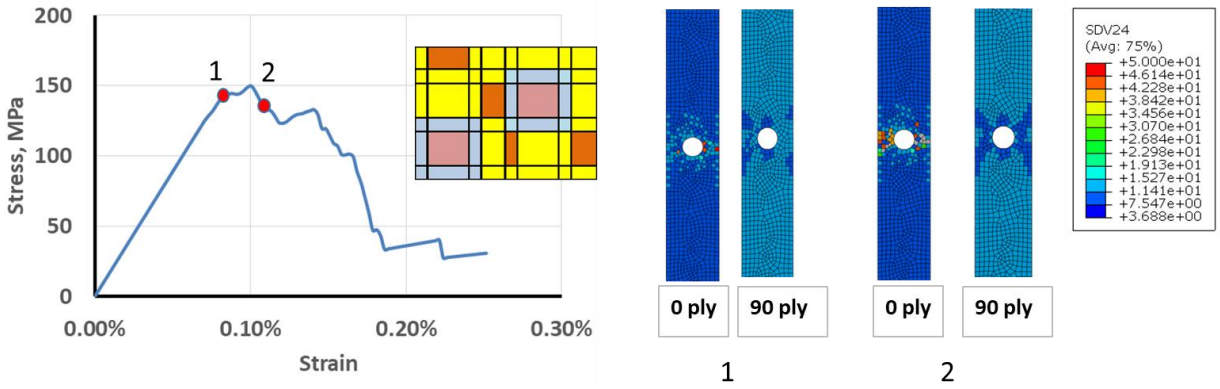

Figure 24 Shows the response of a cross-ply $[0/90]_s$ laminate open-hole test coupon (hole diameter/specimen width = 0.4); A four-phase 6 × 8 RUC used in the analysis is shown in the inset. SDV is a measure of damage.

Figure 25 shows the response of a unidirectional [0] CMC composite double edge notched coupon. This model has 2900 solid 3-D elements with 2 elements through-the-thickness. Analysis took about 5.5 hours of CPU time and multiscale analysis (using the RUC shown in the insert with spatially constant matrix strength) was performed for all elements. As shown in the figure, damage initiation is localized near the notch and the damage progresses towards the center of the coupon as expected. In Figure 25, the damage state is shown on the right side at three stress levels marked 1, 2 and 3.

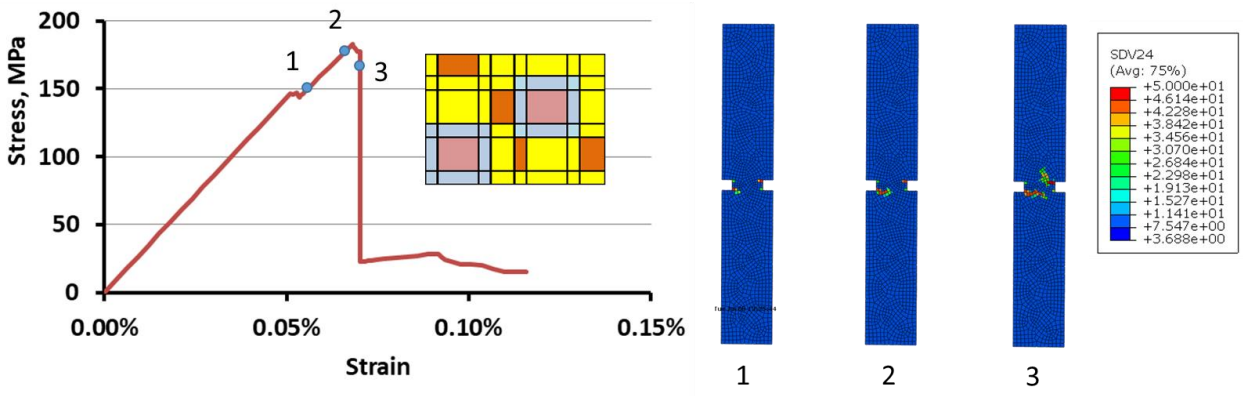

Figure 25 Response of a unidirectional [0] CMC composite double edge-notched coupon (notch width/specimen width = 0.2); A four-phase 6 × 8 RUC used in the analysis is shown in the inset. SDV is a measure of damage.

Macro stress-strain response of both smooth bar (unidirectional and cross-ply) as well as notched specimens were predicted with reasonable efficiency considering that only a single CPU was used to solve the problems. Analyses accounted for residual stresses due to an assumed processing profile and subsequent mechanical analysis. Modeling of notched coupons (open-hole, double-notched) did not involve any additional labor beyond creating the FEA model. Microstructural features (volume fraction, fiber packing, and constituent behavior (both deformation and continuum damage) were included in the FEA constitutive response at each integration point. Results show that damage initiated in the matrix constituent and localized near the notch region as

one would expect. These analyses were performed purely to demonstrate the features and capabilities of the FEAMAC computer code to perform multiscale analyses. Obviously, the density of the FEA mesh affects the results. One would also generate denser meshes near the features of interest such as open holes, notches etc. to better capture stress gradients in those locations. There is always this balance between the fidelity and efficiency of any given analyses. It was also demonstrated, but not shown herein, that multiscale analyses need not be performed over the entire domain of the structure but should be conduct around high stress gradient regions (e.g., within a 2x diameter region of the hole). In this way, the analyses can be conducted even more efficiently without sacrificing the accuracy of the results.

5. Nonlinear Behavior of a Ceramic Matrix Composite Turbine Vane

Ceramic matrix composites (CMCs) are high-temperature materials that are growing in application, particularly for gas turbine engine parts. The purpose of reinforcing a brittle ceramic matrix with a brittle ceramic fiber is to improve the toughness of the material, as opposed to typical polymer matrix composites wherein the fiber serves to improve stiffness and strength. As such, it is important in CMCs to prevent or delay matrix cracks from progressing into the fiber. This is typically accomplished by ensuring a weak interface between the fiber and the matrix in CMCs.

Here a progressive failure simulation of a realistic SiC/SiC CMC turbine vane is demonstrated. This model is intended to exercise NASMAT (which is the next generation HPC version of MAC/GMC and FEAMAC) for a complex geometry [42], but it is not intended to represent a producible component. In this SiC/SiC composite, the fibers are coated with a compliant boron nitride (BN) interface, which has a large enough volume fraction to constitute a third constituent. A CMC with a fiber volume fraction of 0.28 and an interface volume fraction of 0.14 (and matrix volume fraction of 0.58), which is typical of for this composite [1], has been considered. The CMC constituent material properties are given in Table 7, same constituents shown previously in Table 2, but the matrix used here is homogenized version of SiC and silicon; therefore, residual stresses are not captured in this analysis. Unidirectional SiC/SiC composites are commonly used in a cross-ply laminate configuration so that fibers can enhance the toughness in both in-plane directions.

Table 7 Properties of CMC constituent materials.

Property	Hi-Nicalon Type S Fiber	Si/SIC Matrix	BN Interface
Young's Modulus, GPa	385	327	10
Poisson's Ratio	0.17	0.22	0.23
Coeff. Thermal Exp. 10^{-06}/C	3.2	3.2	4.0
Normal Strength, MPa	1800	600	70
Shear Strength, MPa	700	350	45

The FEA of the CMC vane, shown in Figure 26, is adapted from a previous work [43]. It includes an airfoil with a true chord length of 64.8 mm, a z-direction width of 41.9 mm, a suction side wall thickness of 2.03 mm, and a pressure side wall thickness of 1.02 mm. The pressure and suction sides of the airfoil are connected by a rib (with 3.25 mm thickness), resulting in two cavities. Inner and outer bands (71.1 mm by 44.7 mm by 4.06 mm), which are composed of the same CMC material, are also included. The mesh consists of 497,694 C3D10 quadratic tetrahedral elements, with three

integration points per element, with a total of 2,237,235 degrees of freedom. The applied loading, in the form of specified temperatures and a uniform internal cavity pressure is shown in Figure 27 (with no external pressure applied to the airfoil). During the progressive failure simulations, these temperatures and the pressure are ramped up linearly from zero. Fixed boundary conditions are applied to the top and bottom (y-normal) faces of the inner and outer bands, and the model is otherwise free.

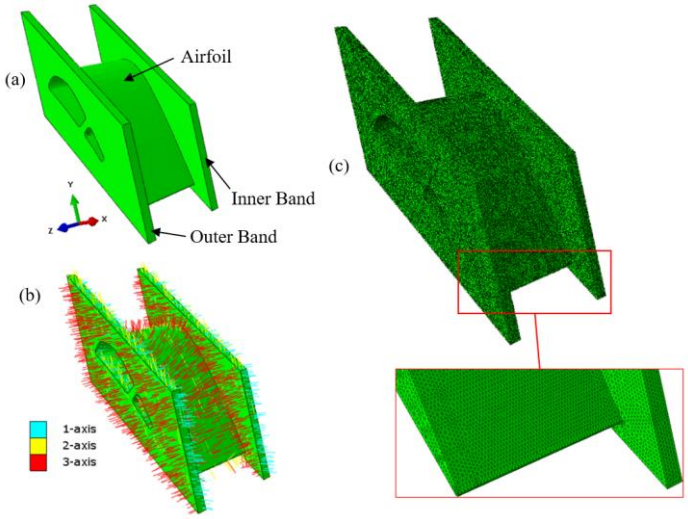

Figure 26 Finite element model of a SiC/SiC CMC vane. (a) Geometry, (b) Material orientations, (c) Mesh.

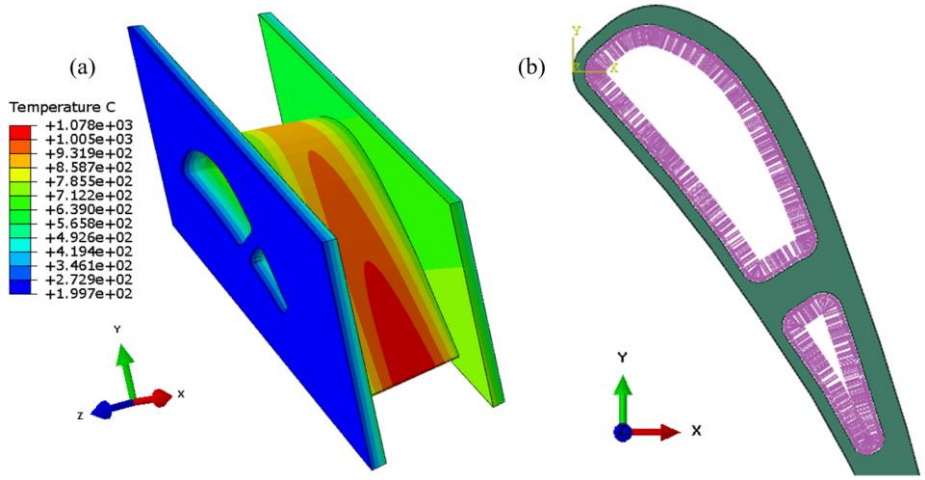

Figure 27 SiC/SiC CMC gas turbine engine vane loading. (a) Applied temperatures, (b) Uniform internal pressure.

The microscale RUC, which operates at every integration point in every element of the FEA, is shown in Figure 28a, and consists of 128 subcells (for a total of 191 million subcells in the 16 multiscale model). This RUC captures the primary features of a cross-ply CMC laminate by including a continuous SiC fiber with a BN coating in both the x1- and x2-directions (which correspond to the 1-axis and 2-axis in Figure 26). This microstructure is homogenized by NASMAT (using the triply periodic version of GMC), and thus provides an effective nonlinear response to the integration points within the FEA. The explicit effects of the individual plies that would make up the vane are

not captured (e.g., residual stress effect). However, this approximation enables the FEA model to be meshed with solid elements without needing to model each ply explicitly. Explicitly modeling the CMC plies with solid elements would obviously increase the number of elements in the FEA dramatically. Of course, alternatively, continuum shell elements could be used to capture the cross-ply layup in the FEA model, in which case a continuous (doubly periodic) RUC would be used at the microscale, but this would not allow for inter-ply damage.

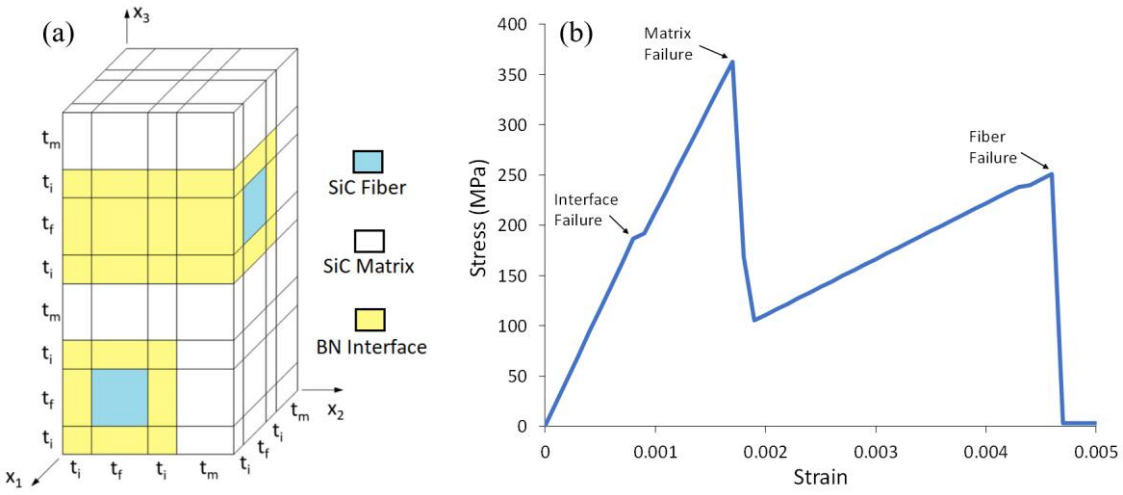

Figure 28 (a) Square-packed triply periodic GMC RUC representation of cross-ply material where subcell dimensions (t_f, t_m, and t_i) are based on constituent's volume fractions (b) Effective in-plane (x_2 or x_3) stress-strain response of RUC.

The subvolume elimination method has been employed at the microscale in the progressive failure simulation. The Hashin failure criterion [44] has been employed for all three constituent materials (where the employed constituent strengths are given in in Table 7). Figure 28b shows the predicted in-plane stress-strain response of the GMC RUC subjected to uniaxial (x2- or x3- direction defined in Figure 28(a)) tension. This provides an example of the homogenized composite material response of each point within the vane FEA. The impact of the constituent material subcell failures on the composite response is clear, with the applicable constituents labeled in the Figure 28b. Although not shown, this composite response agrees well with more detailed micromechanics simulations within a cross-ply SiC/SiC laminate, modeled with classical lamination theory [22]. The simulation was executed on the same HPC system discussed in Section 4.1 using 102 CPUs. The execution took approximately 5.5 hours to complete.

Figure 29 shows a plot of the nodal displacement at a node on the pressure side of the airfoil as a function of the load factor (fraction of total applied thermal and pressure loading). The applicable node is indicated in the inset. The inset also indicates that, over this pressure side, the airfoil bulges outward during the simulation due to applied internal pressure. Ultimately this wall bursts, and the displacement of the node rises rapidly. At the load factor values indicated in Figure 29, plots of the damage patterns are plotted in the subsequent figures.

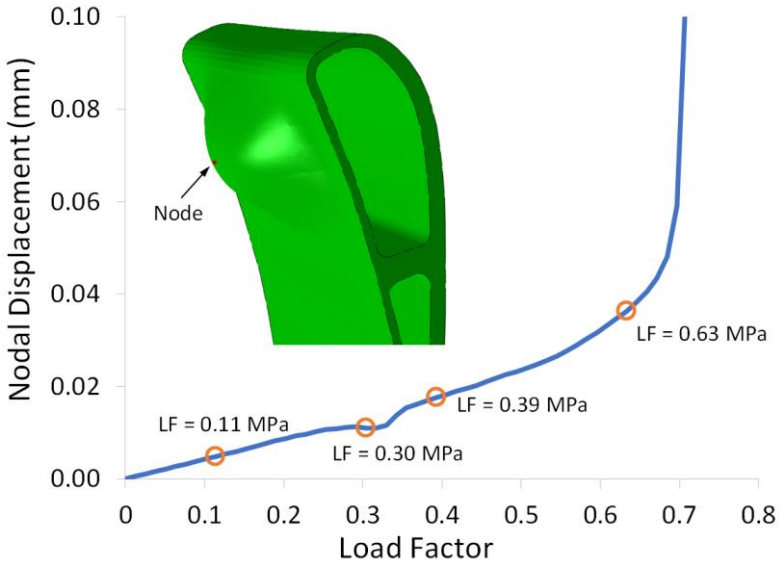

Figure 29 Displacement magnitude vs. applied internal cavity pressure for indicated node on pressure of the airfoil. Plots showing the damage states are given at the indicated load factor (LF) levels.

As indicated in Figure 30, matrix damage initiates at a load factor level of 0.11 at the vane trailing edge at the interface between the airfoil and the end plate. Damage is shown as the number of failed matrix subcells at each element integration point (out of a total of 56 matrix subcells in the RUC, see Figure 28a). Note that some interface subcell failures occur prior to this pressure level, but they have not been shown as their impact on the composite response is minor (Figure 28a). As shown in Figure 31, fiber damage (plotted in the form of number of failed fiber subcells out of a total of 8 in the RUC) initiates in a similar location at a load factor of 0.30, which results in an observable drop in the load carrying capacity of the vane as shown in Figure 29. As the pressure (and temperature) increases, damage progresses along the interfaces between the inner and outer bands of the airfoil. At a load factor of 0.39, see Figure 32, the damage has reached the rib separating the two cavities of the vane. As shown in Figure 32a and b, the matrix damage has progressed through the rib beneath one of the bands and to the suction side of the airfoil. In Figure 32c, fiber damage is shown at a z-cut at the interface of the airfoil and one band. There is also considerable fiber damage at the airfoil trailing edge. At this applied pressure, as shown in Figure 32, interface damage (plotted as the number of failed interface subcells out of a total of 64 in the RUC) is considerable.

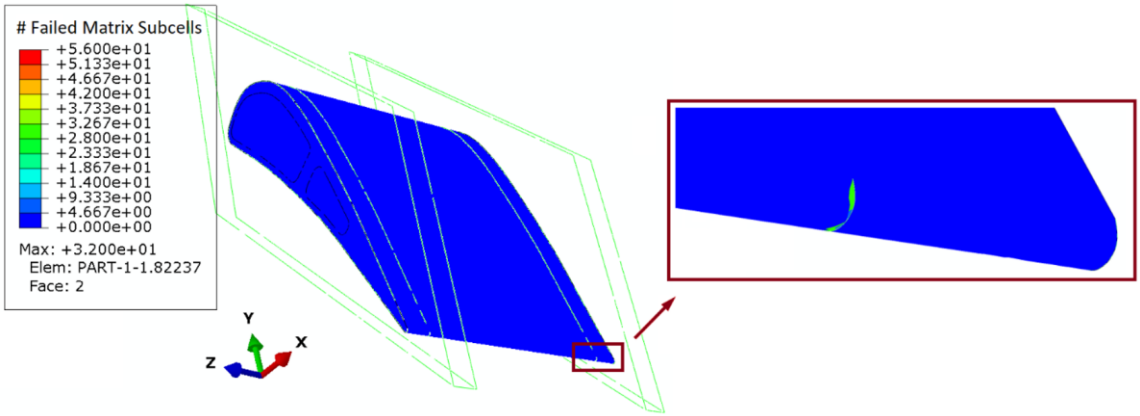

Figure 30 Matrix damage (number of failed subcells per RUC at each integration point) at a load factor level of 0.11 in the CMC vane progressive failure simulation.

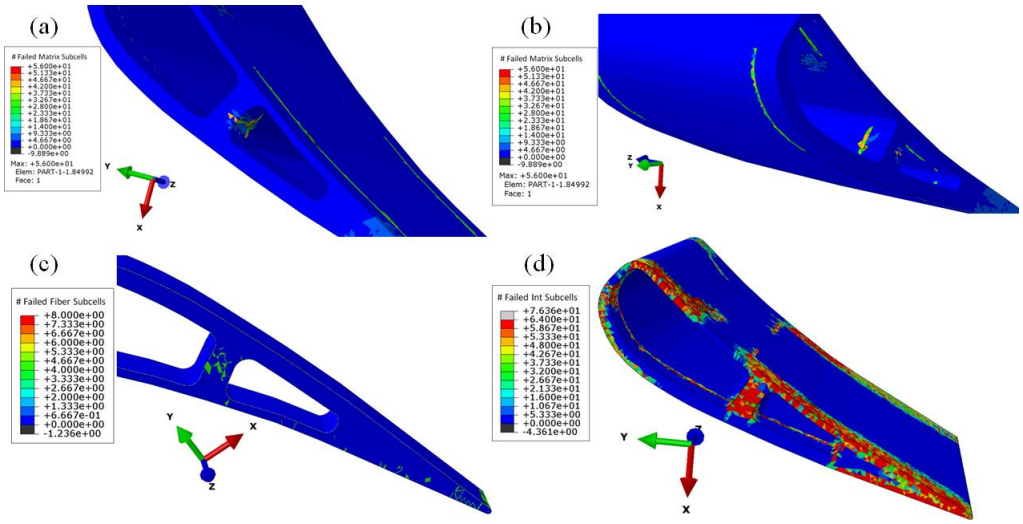

Figure 31 Fiber damage (number of failed subcells per RUC at each integration point) at a load factor level of 0.30 in the CMC vane progressive failure simulation.

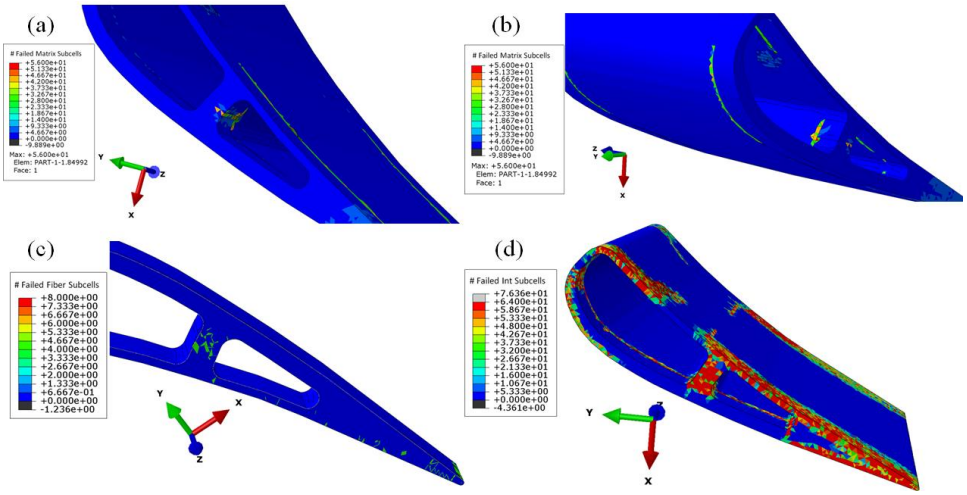

Figure 32 Local failures at a load factor level of 0.39 in the CMC vane progressive failure simulation. (a) and (b) Matrix damage, (c) Fiber damage (a z-cut at the interface of the airfoil and one end plate is shown). (d) Interface damage.

Between load factors of 0.39 and 0.63 (see Figure 29) the displacement of the plotted node begins to increase nonlinearly. Figure 33 shows the matrix and fiber damage at load factor of 0.63. There is substantial matrix damage across the pressure side of the airfoil and the nodal displacement plotted in Figure 29 is increasing rapidly, indicating likely failure of the part. Note that, because the CMC fibers are in the x1-x2 plane, see Figure 28a, this type of pressure-induced out-of-plane failure can occur without causing failure of all the fibers.

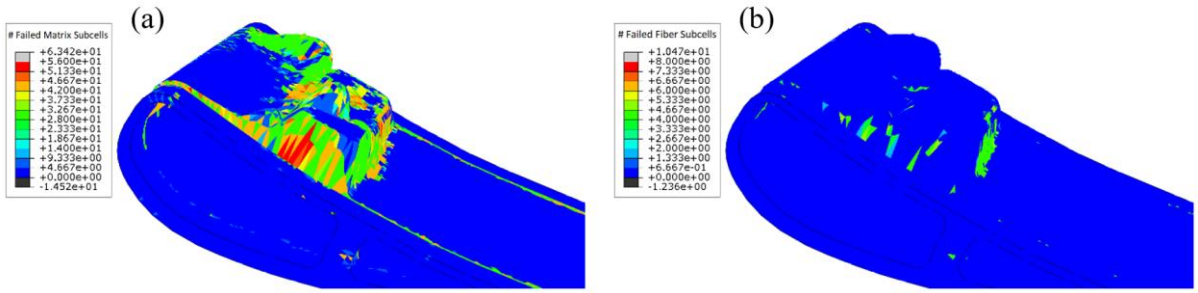

Figure 33 Local failures at a load factor of 0.6 in the CMC progressive failure simulation (plotted on deformed geometry). (a) Matrix damage, (b) Fiber damage.

6. Discussion

CMC response is affected by residual stresses that arise during the processing of composites and manufacturing processes which produce internal material microstructures. The use of micromechanics is important to properly account for any constituent creep/relaxation behavior that takes place during the processing of composites. One can account for residual stresses in an approximate manner (via artificial CTE parameterization) for faster analyses; however, such an approach inhibits accounting for redistribution of residual stresses due to time-dependent effects such as post processing heat treatment performed subsequently or merely time at temperature during creep and relaxation loading. It was also shown that in general, inclusion of residual stresses increases the PLS and thus increases the stress allowable for the composite. However, with this increase in PLS a commensurate decrease in composite ultimate tensile strength is observed due to increases in fiber pre-straining.

Integrated computational materials engineering (ICME) is an integrated approach to the design of products and the materials that comprise them by linking material models at multiple time and length scales. In this paper the statistical influence of microstructure (both ordered and disordered) on the unidirectional and laminated composite effective properties, PLS and fatigue life was investigated for the case of ceramic matrix composites with compliant interfaces. In addition, the advantages/limitations of the micromechanics idealization (GMC or HFGMC) available within the general, synergistic, multiscale-modeling framework for composites (developed by the NASA Glenn Research Center (GRC) and known as MAC/GMC, FEAMAC and most recently NASMAT) when considering microstructural arrangement was discussed. The important findings are summarized:

a) Accounting for spatial variations in composite microstructure within the RUC analyzed is important, as these variations can account for observed statistical variations in both effective properties, PLS and fatigue life.
b) Both micromechanics idealizations can be used to account for this variation; however, the more computationally efficient Generalized Method of Cells (GMC) is significantly more

sensitive to microstructure variations, because of the presence of the compliant interface and lack of normal/shear coupling, than is the High Fidelity Generalized Method of Cells (HFGMC).

i. HFGMC has subcell discretization dependence while GMC does not.
ii. HFGMC typically predicted higher effective properties, PLS, and lower (higher in the case of disordered) fatigue lives than did GMC for order and disordered microstructures.
iii. HFGMC ordered - hexagonal fiber packing – provides excellent agreement with the mean values resulting from disordered microstructures for most of the effective properties. However, for failure (PLS and fatigue lives) HFGMC hexagonal fiber packing over estimated mean results of 100 random instances by approximately 30% for [90] and 20% for $[0/90]_S$ layups. Thus, indicating the need to address disordered microstructures (obtain accurate local fields) when desiring to accurately predict failure of composites.
iv. Although the fatigue lives predicted by HFGMC and GMC can vary significantly based on individual microstructures, the mean fatigue life value (i.e., averaged over multiple microstructure realizations) for a given RUC discretization (e.g., 4 (20 × 20) fiber unit cells within the RUC) between HFGMC and GMC is relatively small (<30%). Note, that the actual percentage discrepancy, in the case of disordered microstructures, is highly dependent upon volume fraction and property mismatch between constituents.

c) Transversely loaded unidirectional composites, [90], demonstrated the highest sensitivity to microstructure, whereas for laminates with [0] plies, e.g. $[0/90]_S$, this sensitivity greatly suppressed.
d) Variability in fiber diameter and interface coating had little to no impact on shifting the mean response of an identical composite system with a constant fiber diameter and coating thickness – provided the fiber and interface volume fraction remained fixed.
e) Periodic ordered hexagonal pack RUC approximated the mode of the non-normal distribution resulting from disordered microstructures reasonably well and thus enables a more computationally efficient use of microstructures for design purposes.

A few multiscale analyses were also shown using simple, ordered RUCs to demonstrate that micromechanics-based solutions can be performed in reasonable time to provide engineering solutions. Clearly, micromechanics can be effectively utilized to link the material microstructure (e.g., constituent phase properties, volume fraction, fiber packing (ordered or disordered), etc.) to ply/laminate properties (mesoscale) and finally to performance (at the macroscale), in an efficient and accurate manner to enable 'fit-for-purpose' tailoring of the composite material. The ability to localize and homogenize efficiently between scales make MAC/GMC and FEAMAC ideal candidates for ICME simulations in a multiscale environment in which the microstructure can be optimized spatially based on the local loading and environmental history. Finally, extreme caution should be used when adopting/utilizing input constituent (fiber/matrix) properties either from the literature or a given model, as the fidelity of the given model used to obtain those "in-situ material properties" will impact the predictive ability of another model with a different degree of fidelity and assumptions. The NASA Multiscale Analysis Tool (NASMAT) software has proven capable of performing engineering analysis of composite materials and structures using HPC. It enables the consideration of an arbitrary number of material microstructural length scales, plugs in to standard finite element software to provide the nonlinear effective composite material response. Herein, it was demonstrated that NASMAT can indeed solve industry size multiscale problems as

demonstrated by the analysis of a [0/90] SiC/SiC vane comprising of 2.4 million DOF along with concurrent simulation of 245 million total number of subcells at each time step. The total progressive damage analysis took 5.5 hours using 102 CPUs with parallelization at highest (FEA) scale. The size of the multiscale problems can be prohibited by memory requirements. Currently, the focus of NASMAT development is to improve memory management without sacrificing computational speed as well as parallelization of the multiscale micromechanics methods in the code [45].

Author Contributions

Dr Mital contributions were associated with producing most results and writing manuscript. Dr. Arnold was responsible for project development, reviewing results and writing manuscript. Dr. Bednarcyk and Dr. Pineda contributed to the FEA CMC vane results and were primary software developers.

Competing Interests

The authors have declared that no competing interests exist.

References

1. Dunn D. The effect of fiber volume fraction in HiperComp® SiC-SiC composites. Alfred, NY: Alfred University; 2010.
2. Bednarcyk BA, Arnold SM. MAC/GMC 4.0 user's manual, volume 2: Keywords manual. Hanover, MD: NASA Center for AeroSpace Information; 2002; TM 2002-212077/Vol 2.
3. Pineda EJ, Bednarcyk BA, Ricks TM, Arnold SM, Henson G. Efficient multiscale recursive micromechanics of composites for engineering applications. Int J Multiscale Comput Eng. 2021; 19: 77-105.
4. Sorini C. Multiscale modeling of polymer and ceramic matrix composites. Tempe, AZ: Arizona State University; 2021.
5. Skinner TD, Chattopadhyay A. Multiscale thermomechanical damage model with internal state variables for ceramic matrix composites. Proceedings of the AIAA Scitech 2020 Forum; 2020 January 6th-10th; Orlando, FL, USA. Reston: American Institute of Aeronautics and Astronautics.
6. Meyer P, Waas AM. FEM predictions of damage in continuous fiber ceramic matrix composites under transverse tension using the crack band method. Acta Mater. 2016; 102: 292-303.
7. Chateau C, Gélébart L, Bornert M, Crépin J. Micromechanical modeling of the elastic behavior of unidirectional CVI SiC/SiC composites. Int J Solids Struct. 2015; 58: 322-334.
8. Katoh Y, Snead LL, Henager Jr CH, Nozawa T, Hinoki T, Iveković A, et al. Current status and recent research achievements in SiC/SiC composites. J Nucl Mater. 2014; 455: 387-397.
9. Zok FW. Fracture analysis of fiber-reinforced ceramic-matrix composites. In: ASM handbook. Materials Park, OH: ASM International; 2001. pp. 407-418.
10. Baig M, Owusu-Danquah J, Campbell AA, Duffy SF. Inelastic constitutive modeling: Polycrystalline materials. Materials. 2023; 16: 3564.
11. Shojaei A, Li G, Fish J, Tan PJ. Multi-scale constitutive modeling of ceramic matrix composites by continuum damage mechanics. Int J Solids Struct. 2014; 51: 4068-4081.

12. Mseis G. Multiscale modeling and homogenization of composite materials. Berkeley, CA: Department of Mechanical Engineering, University of California; 2010.
13. Liu X, Furrer D, Kosters J, Holmes J. Vision 2040: A roadmap for integrated, multiscale modeling and simulation of materials and systems. Hanover, MD: NASA Center for AeroSpace Information; 2018; NASA/CR-2018-219771.
14. Skinner T, Chattopadhyay A. Multiscale temperature-dependent ceramic matrix composite damage model with thermal residual stresses and manufacturing-induced damage. Compos Struct. 2021; 268: 114006.
15. Nadabe T, Takeda N. Numerical analysis on effect of random fiber arrangement for transverse compressive strength of fiber reinforced composites. Proceedings of the 8th China CAE Annual Conf. and 201222 National Symposium for Advanced CAE Technology and Application; 2012 July 26th-27th; Chengdu, China. Beijing: The Chinese Society of Theoretical and Applied Mechanics.
16. Trias D, Costa J, Turon A, Hurtado JE. Determination of the critical size of a statistical representative volume element (SRVE) for carbon reinforced polymers. Acta Mater. 2006; 54: 3471-3484.
17. Huang Y, Jin KK, Ha SK. Effects of fiber arrangement on mechanical behavior of unidirectional composites. J Compos Mater. 2008; 42: 1851-1871.
18. Maligno AR, Warrior NA, Long AC. Effects of inter-fibre spacing on damage evolution in unidirectional (UD) fibre-reinforced composites. Eur J Mech A Solids. 2009; 28: 768-776.
19. Wang Z, Wang X, Zhang J, Liang W, Zhou L. Automatic generation of random distribution of fibers in long-fiber-reinforced composites and mesomechanical simulation. Mater Des. 2011; 32: 885-891.
20. Romanov V, Lomov SV, Swolfs Y, Orlova S, Gorbatikh L, Verpoest I. Statistical analysis of real and simulated fibre arrangements in unidirectional composites. Compos Sci Technol. 2013; 87: 126-134.
21. Garnich M, Fertig RS, Anderson EM. Random fiber micromechanics of fatigue damage. Proceedings of the 54th AIAA/ASME/ASCE/AHS/ASC structures, structural dynamics, and materials conference; 2013 April 8th-11th; Boston, MA, USA. Reston: American Institute of Aeronautics and Astronautics.
22. Arnold SM, Murthy PL, Bednarcyk BA, Pineda EJ. Microstructural influence on deformation and fatigue life of composites using the generalized method of cells. Proceedings of the 56th AIAA/ASCE/AHS/ASC Structures, Structural Dynamics, and Materials Conference; 2015 January 5th-9th; Kissimmee, FL, USA. Reston: American Institute of Aeronautics and Astronautics.
23. Aboudi J, Arnold SM, Bednarcyk BA. Micromechanics of composite materials: A generalized multiscale analysis approach. Oxford: Butterworth-Heinemann; 2013.
24. Paley M, Aboudi J. Micromechanical analysis of composites by the generalized cells model. Mech Mater. 1992; 14: 127-139.
25. Aboudi J, Pindera MJ, Arnold SM. Higher-order theory for periodic multiphase materials with inelastic phases. Int J Plast. 2003; 19: 805-847.
26. Liu KC, Ghoshal A. Inherent symmetry and microstructure ambiguity in micromechanics. Compos Struct. 2014; 108: 311-318.
27. Aboudi J, Arnold SM, Bednarcyk BA. Practical micromechanics of composite materials. Oxford: Butterworth-Heinemann; 2021.

28. Dowling NE. Mechanical behavior of materials: Engineering methods for deformation, fracture and Fatigue. Upper Saddle River, NJ: Prentice Hall; 1999.
29. Lemaitre J, Chaboche JL. Mechanics of solid materials. Cambridge: Cambridge University Press; 1990.
30. Skrzypek J, Hetnarski R. Plasticity and creep theory examples and problems. Boca Raton, FL: CRC Press; 1993.
31. Odqvist FK. Theory of creep under the action of combined stresses with applications to high temperature machinery. Stockholm: Generalstabens litografiska anstalts förlag; 1936.
32. Yang Z, Pei C, Yan H, Long L. Fatigue damage modeling of ceramic-matrix composites: A short review. Mat Design Process Comm. 2020; 2: e129.
33. Kim TT, Mall S, Zawada LP. Fatigue behavior of Hi-Nicalon Type-S™/BN/SiC ceramic matrix composites in a combustion environment. Int J Appl Ceram Technol. 2011; 8: 261-272.
34. Arnold SM, Kruch S. Differential continuum damage mechanics models for creep and fatigue of unidirectional metal matrix composites. Int J Damage Mech. 1994; 3: 170-191.
35. Chaboche JL, Lesne PA. A non-linear continuous fatigue damage model. Fatigue Fract Eng Mater Struct. 1988; 11: 1-17.
36. Wilt TE, Arnold SM, Saleeb AF. A coupled/uncoupled computational scheme for deformation and fatigue damage analysis of unidirectional metal-matrix composites. In: Applications of continuum damage mechanics to fatigue and fracture. West Conshohocken, PA: ASTM; 1997. pp. 65-82.
37. Kruch S, Arnold SM. Creep damage and creep-fatigue damage interaction for metal matrix composites. In: Applications of continuum damage mechanics to fatigue and fracture. West Conshohocken, PA: ASTM; 1997. pp. 7-28.
38. Hansen L. Behavior of SiC-SiC composite laminates under multiaxial load states: Experiments and simulations. Ann Arbor, MI: University of Michigan; 2015.
39. Murthy PL, Bednarcyk BA, Mital SK. A compilation of MATLAB scripts and functions for MACGMC analyses. Hanover, MD: NASA Center for AeroSpace Information; 2017; NASA/TM/2017-219500.
40. Naghipour Ghezeljeh P, Arnold SM, Pineda EJ, Stier B, Hansen L, Bednarcyk BA, et al. Multiscale static analysis of notched and unnotched laminates using the generalized method of cells. Hanover, MD: NASA Center for AeroSpace Information; 2016; NASA/TM-2016-219084.
41. Hilmas AM, Henson G, Singhal A, Gao Y, Schuster M. In-situ observation of damage in unidirectional CMC laminates under tension. Ceram Int. 2020; 46: 13502-13510.
42. Pineda EJ, Ricks TM, Bednarcyk BA, Arnold SM. Software architecture and hierarchy of the NASA multiscale analysis tool. Proceedings of the 2020 Conference on Advancing Analysis & Simulation in Engineering; 2020 Jun 16th-18th; Indianapolis, IN, USA. Cleveland: NASA Glenn Research Center.
43. Boyle RJ, Parikh AH, Nagpal VK. Design concepts for cooled ceramic composite turbine vane. Hanover, MD: NASA Center for AeroSpace Information; 2015; NASA/CR-2015-218390.
44. Hashin Z. Failure criteria for unidirectional fiber composites. Int J Appl Mech. 1980; 47: 329-334.
45. Kaleel I, Ricks TM, Gustafson PA, Pineda EJ, Bednarcyk BA, Arnold SM. Massively multiscale modeling using NASA multiscale analysis tool through partitioned task-parallel approach. Proceedings of the AIAA SCITECH 2023 Forum; 2023 January 23rd-27th; National Harbor, MD, USA. Reston: American Institute of Aeronautics and Astronautics.